Using remote sensed actual evaporation to improve hydrological models

Master Thesis for the degree of Master of Science in Civil Engineering at Delft University of Technology

Author: Bart Schilperoort

RO 0713.10 August 31, 2016

HKV CONSULTANTS

Abstract

In hydrological models evaporation is often still quite uncertain. Potential evaporation is used as input, but the modelling of plant stresses is not always accurate enough to describe the behaviour in reality. In situ measured actual evaporation data is rare, and doing measurements is time consuming and expensive. With the advance of satellite technology, remote sensing products modelling actual evaporation have been developed. To see if models can be easily improved using this actual evaporation data, it will be directly imposed.

As remote sensing data product, the LSA SAF actual evaporation product will be used. As input it uses most importantly Meteosat-10 data. As other sources it has ERA-interim and ECOCLIMAP. Accuracy is generally high when comparing it to in situ measurements ($R^2 = 0.90$ when comparing it to eddy covariance at Cabauw), although a correction factor might be necessary for some locations. Three models were tested, WALRUS, SIMGRO and FLEX. Two sites in the Netherlands were studied (Cabauw and the Hupsel Brook) and two catchments in Spain (Ubierna and Ulzama). WALRUS was applied to the Cabauw Polder and the Hupsel Brook, SIMGRO was applied to Cabauw, and FLEX was used in Spain.

SIMGRO did not perform well, and modelled water stress during summers at Cabauw, while in situ measurements showed that water stress was not an issue. The performance was too low for LSA SAF evaporation to make a difference. WALRUS performed well at Cabauw, although there was no difference between the performance of the model when using actual evaporation instead of Makkink evaporation (NS=0.693 and NS=0.673 respectively), as the catchment does not suffer from water stress. In the Hupsel Brook water stress does occur, and the model performs slightly better when using actual evaporation instead of Makkink evaporation (NS=0.762 and NS=0.733 respectively). In Spain the uncertainty of the input data was high, and some corrections were necessary. For the Ubierna catchment, the performance was clearly better with the LSA SAF actual evaporation instead of the Makkink evaporation (log-NS=0.787 and log-NS=0.698). For the Ulzama catchment the model using LSA SAF actual evaporation also performed better than the Makkink evaporation (log-NS=0.769 and log-NS=0.708).

These results show that the LSA SAF product can give a good representation of actual evaporation, and that directly using it in hydrological models can improve their performance if the vegetation in the catchment experiences water stress.

Acknowledgements

First and foremost I would like to thank my daily supervisors Rudolf Versteeg and Miriam Coenders for their support throughout the last eight months. With their help I have learned more about the many methods for measuring and determining evaporation, along with all the ins and outs of hydrological models.

I would also like to thank Claudia Brauer for the WALRUS model and the help she provided me with. Additionally, I would like to thank Ab Veldhuizen for his help with understanding the SIMGRO model, and Joost Heijkers for providing me with the HDSR SIMGRO model.

Lastly I would like to thank Fred Bosveld & Claudia Brauer for the *Cabauw experimental site for atmospheric research* database, which provided me with a large amount of data of the Cabauw site.

Contents

List of Figures

List of Tables

1 Introduction

1.1 Measuring and calculating evaporation

Evaporation is a key process in the hydrological cycle (Zhao et al., 2013), and is very important for hydrological models. After precipitation, evaporation data is the main input required.

Evaporation on a given location can be determined in several ways, each with its own assumptions and (generally large) inaccuracies. It is either determined by making measurements, or by using models. The current standard for measuring evaporation is eddy covariance (Burba, 2013), which measures the net water vapour rising up in the atmosphere. Previously the Bowen ratio energy balance method (Bowen, 1926) was mainly used, which derives evaporation using the vertical gradients of temperature and water vapour in the atmosphere, combined with closing a local energy balance. For models, mainly potential evaporation is used, usually the Penman-Monteith (Allen et al., 1998) or Makkink (Hooghart and Lablans, 1988) equations. These require meteorological input to get to the evaporation of a well-watered standard crop. Internationally Penman-Monteith is the most used equation, but in the Netherlands Makkink is still mostly used. The discussion on which one should be used is still going on (Droogers, 2009), but as most models (in the Netherlands) still have Makkink as default reference evaporation it will be used in this study.

In this study evaporation is defined as the total evaporation from all sources (plant transpiration, interception evaporation, soil evaporation and open water evaporation). Actual evaporation is the evaporation which is taking place in reality, in contrast to potential evaporation which is the evaporation under ideal conditions (without water stress limiting the transpiration of vegetation) (Maidment, 1993). When measuring and calculating evaporation, generally the energy flux of evaporation is given (latent heat flux). To convert this to evaporation expressed in water depth over time (mm/d) the latent heat flux has to be multiplied by the latent heat of vaporization of water.

1.1.1 Eddy covariance

Eddy covariance is based on measuring the 3D wind speed in high frequency, along with the water vapour in and temperature of the air. The method assumes that all vapour and heat is transferred turbulently in large and small scale eddies (Figure 1-1). By analysing the vertical (both upward and downward) transport of vapour and heat, the latent and sensible heat fluxes can be determined.

Figure 1-1 Representation of eddies passing a measurement tower (Burba, 2008)

The method relies on the assumption that the atmospheric fluxes are fully turbulent, the upwind footprint represents the measurement area, and that terrain is horizontal and uniform. Forced convection (where wind transports heat from the surface) also has to dominate over natural convection

(where warm air rises due to buoyancy).

As these assumptions are not always valid, the method suffers from the non-closure of the energy balance (Foken, 2008), where the net energy from solar radiation is higher (or lower) than the sum of the eddy covariance fluxes and the storage fluxes:

$$R_N = H_{EC} + LE_{EC} + G_{total} \tag{1-1}$$

Where R_N is the net radiation (W/m^2), LE$_{\mathrm{EC}}$ the eddy covariance measured latent heat flux (W/m^2), H_{EC} the eddy covariance measured sensible heat flux (W/m^2), and G_{total} the storage term (representing the soil, canopy, and other heat fluxes) (W/m^2). Usually eddy covariance underestimates the latent and sensible fluxes (Wilson, 2002). The net radiation is locally measured using a radiometer, and the heat flux terms are generally measured using heat flux plates and thermocouples.

At the measurement tower at Cabauw, the KNMI uses two different methods to determining the evaporation (Bosveld, 2014). The main method used is the energy balance method, where latent heat of evaporation is the leftover flux after determining the other terms:

$$LE_1 = R_N - G_S - H_{EC} \tag{1-2}$$

Where LE_1 is the latent heat flux of method 1 (W/m^2), and G_S the measured soil heat flux (W/m^2). The assumption in this method is that all energy missing from the energy balance is evaporation. While the site at Cabauw has well wetted grass as land cover (meaning most energy is used for evaporation), research shows that this assumption is false, as eddy covariance underestimates all fluxes and not just latent heat (Twine et al., 2000).

The second method is to use the Bowen ratio to split up the remaining energy between the latent and sensible heat fluxes, the most accurate according to Wolf et al. (2008). As the Bowen ratio is the ratio between the sensible and latent heat flux, the eddy covariance flux ratio is used:

$$\beta_{EC} = \frac{H_{EC}}{LE_{EC}} \tag{1-3}$$

Where β_{EC} is the eddy covariance measured Bowen ratio (-). Using the Bowen ratio the latent heat flux of method 2 (LE_2, W/m^2) can then be determined from the available energy:

$$LE_2 = \frac{R_N - G}{1 + \beta_{EC}} \tag{1-4}$$

Eddy covariance measurement datasets are scarce (Oak Ridge National Laboratory Distributed Active Archive Center (ORNL DAAC), 2016), especially if processed and gap filled data is needed. The only locations in the Netherlands where measurements are consistently done and available are at Cabauw (polders, south-western Utrecht) and at Loobos (evergreen coniferous forest, western side of the Veluwe).

1.1.2 Bowen ratio

The Bowen ratio energy balance method is based on the theory of I.S. Bowen which describes the ratio of sensible heat to latent heat rising in the atmosphere with the temperature and vapour pres-

sure gradients (Bowen, 1926):

$$\beta = \frac{H}{\mathrm{LE}} = \gamma \frac{\Delta T_a}{\Delta e_a} \tag{1-5}$$

Where β is the Bowen ratio (-), γ the psychrometric constant (kPa/ °C), ΔT_a the gradient of the air temperature over the height (°C) and Δe_a the gradient of the vapour pressure of water over the height (kPa). LE is the latent heat of evaporation (W/m^2) and H the sensible heat (W/m^2).

ΔT_a and Δe_a can be determined by using a psychrometer (wet-and-dry-bulb thermometer), on at least two different heights. To then calculate the latent heat flux, completing the energy balance is necessary:

$$LE = \frac{R_N - G_{\mathrm{total}}}{1+\beta} \tag{1-6}$$

Just as with eddy covariance, the Bowen ratio method only measures fluxes at times when forced convection dominates. When closing the energy balance it is assumed that the energy which is transported due to mainly natural convection has the same ratio of latent heat to sensible heat.

1.1.3 Other methods of measuring actual evaporation

Other methods for measuring local evaporation are the lysimeter, scintillometer and the similarity model of Monin and Obukhov.

A lysimeter is where an excavated part of the soil is put on a dug-in scale, and treated like the surrounding area (Allen et al., 1998). With this the effect of evaporation can be measured by the change of weight of the soil column, but the method can have problems with representing the surrounding area due to the lack of capillary rise from below and the disturbance of the soil. It is also expensive and invasive.

The scintillometer works by deriving the sensible heat flux from small fluctuations of the refractive index of air (caused by differences in temperature, humidity and pressure) (Meijninger et al., 2006). The latent heat flux can then be derived using the energy balance.

Lastly, the similarity model of Monin and Obukhov allows for estimating the sensible heat flux from the vertical temperature and wind speed profiles (Stricker and Brutsaert, 1978). Just like the eddy covariance method, the model depends on forced convection being dominant.

1.1.4 Penman-Monteith

The Penman-Monteith equation is used around the world to calculate reference evaporation, and is regarded as the most accurate one for a wide variety of climatic conditions (Allen et al., 1998). It takes into account both available energy and aerodynamic terms to calculate the reference evaporation, the amount of water evaporated by a reference crop under ideal conditions. The equation is defined as follows (Allen et al., 1998):

$$LE = \frac{s\,(R_n - G) + \rho_a c_p \frac{e_s - e_a}{r_a}}{s + \gamma\left(1 + \frac{r_a}{r_s}\right)} \tag{1-7}$$

Where LE is the latent heat of evaporation (W/m^2), R_n is the net radiation (W/m^2), G the ground heat flux (W/m^2), ρ_a the air density (kg/m^3), c_p the specific heat of the air (J/kg/ °C), e_s the saturation vapour pressure (kPa), e_a the actual vapour pressure (kPa), s the slope of the saturation

vapour pressure curve at the air temperature (kPa/ °C), γ the psychrometric constant (kPa/ °C), r_a the aerodynamic resistance (s/m), and r_s the surface resistance (s/m).

1.1.5 Makkink equation

For short well-watered grass, Makkink formulated a simplified equation to calculate the evaporation (Hooghart and Lablans, 1988). The equation is based on the equation of Penman-Monteith, but neglecting the influence of ground heat flux, and the wind and vapour deficit related terms:

$$LE = c_1 \frac{s}{s+\gamma} R_{S\downarrow} + c_2 \tag{1-8}$$

Where $R_{S\downarrow}$ is the incoming shortwave radiation (W/m^2), and c_1 and c_2 are empirical constants. From field tests with grass, values for c_1 and c_2 were determined, where $c_1 = 0.65$ and $c_2 = 0$ performed very well. This leads to the formula for Makkink reference evaporation:

$$LE_{\text{ref}} = 0.65 \frac{s}{s+\gamma} \frac{R_{S\downarrow}}{\lambda} \tag{1-9}$$

Neglecting the influence of the ground heat flux, wind and vapour deficit terms generally leads to an underestimation during summer and an overestimation during winter when comparing the Makkink equation to the full Penman-Monteith equation (Hooghart and Lablans, 1988).

1.2 Problem definition

In most existing rainfall runoff models potential evaporation is used as input to estimate the actual evaporation taking place. This potential evaporation needs to be reduced at times when plants suffer from water related stresses (Allen et al., 1998). Different models use different methods, ranging from calculating the head in the unsaturated zone in which the plants are rooted, to relating the reduction to a moisture shortage in the unsaturated zone (Feddes et al., 1978). If the assumptions which are used are incorrect, or if the soil parameters are not in accordance to reality, this evaporation reduction can differ from reality.

Errors in evaporation estimates might not be immediately visible since direct observations are limited, or if only the discharge and groundwater levels are looked at when calibrating or verifying the model. This means that essential processes might be missed and that the model does not perform optimally or realistically, a problem related to 'getting the right answer to for the wrong reason' (Kirchner, 2006).

Before the advancements in satellite technology getting actual evaporation measurements took a lot of effort and could only be done locally. The time intensive Bowen ratio method was used until the rise of the eddy covariance method in the late 1980s (Burba, 2013). Eddy covariance systems allow for more continuous evaporation measurements, but can easily exceed research budgets and as such are not frequently used.

To accommodate the demand for more information on evaporation, methods have been established to estimate actual evaporation using satellite data, for example SEBAL (Bastiaanssen et al., 1998) and MODIS (Mu et al., 2007). The direct algorithms will only work during cloudless skies however, as the satellites need vision of the ground. To circumvent this problem extensive meteorological models are used to fill in the data gaps caused by cloud cover. These products can offer spatially distributed evaporation data in a way local measurements cannot. However, their accuracy is lower and the uncertainty is higher compared to local measurements.

1.3 Research Questions

The problems with using potential evaporation (Bartholomeus and Witte, 2013) and the availability of data products for spatially distributed actual evaporation leads to the research questions:

How does satellite actual evaporation compare to ground measurements?

And how well do models perform when imposing actual evaporation?

This research questions will be investigated by first comparing the remote sensing based actual evaporation to local measurements, and then looking at the performance of existing hydrological models, and comparing it to the performance while actual evaporation is imposed. The product used in this study is the LSA SAF actual evaporation product, a free open data product based on EUMETSAT data (LSA SAF, 2010). Two locations will be studied in the Netherlands, but as evaporation generally is not limited by water availability in the Netherlands, a flexible conceptual model will be used on arid catchments in Spain.

1.4 Report structure

In Chapter 2 the LSA SAF actual evaporation algorithm will be explained, the study sites will be described and the used model structures are explained. In Chapter 3 a comparison between the LSA SAF actual evaporation and local measurements will be made. In Chapter 4 the results of imposing actual evaporation on the models will be shown and discussed. Discharge performance comparisons between Makkink and actual evaporation as input will be made using the Nash-Sutcliffe model efficiency. In Chapter 5 the results will be globally discussed, and what their implications are. In Chapter 6 the conclusions of the study will be given.

2 Methodology and site descriptions

2.1 LSA SAF actual evaporation

The Land Surface Analysis Satellite Applications Facility (LSA SAF) has as goal to increase the benefit of EUMETSAT satellite data related to land, land-atmosphere interaction and the biosphere. It provides freely and openly available data products such as leaf area index, surface albedo, downward surface radiation fluxes and also actual evaporation. LSA SAF is a consortium of the Portuguese, French and Belgian meteorological institutes, along with the Karlsruhe Institute of Technology, the University of Lisbon, the University of Valencia, King's College London and VITO. IPMA, the Portuguese meteorological institute is the leader of the consortium. In this study only the daily actual evaporation product will be used.

2.1.1 Data sources

The LSA SAF evaporation algorithm gets its data from many sources (Figure 2-1). First the data of the geostationary Meteosat-10 (in case of a clear sky), which provides the incoming radiation, albedo, leaf area index and fraction of vegetation within a tile. From the satellite based ECOCLIMAP it retrieves the land use, albedo, emissivity, stomatal resistance and roughness length every month. Finally the ERA-interim climate reanalysis provides air temperature, dew point temperature, precipitation and soil moisture estimates.

If the Meteosat-10 satellite does not have a clear view of the sky, the ECOLIMAP albedo will be used instead. The LSA SAF downward radiation fluxes ($R_{S\downarrow}$ and $R_{L\downarrow}$) are still estimated when clouds block the view. The downward shortwave radiation is based on a simplified physical description of the radiation transfer in the cloud-atmosphere-surface system (LSA SAF, 2012). The downward longwave radiation uses a scheme which is applicable in both cloudy and non-cloudy situations (LSA SAF, 2009). As the leaf area index (LAI) and fraction of vegetation cover (F_{veg}) observations are valid for a longer time, the high quality observations (cloud free) are used to determine those.

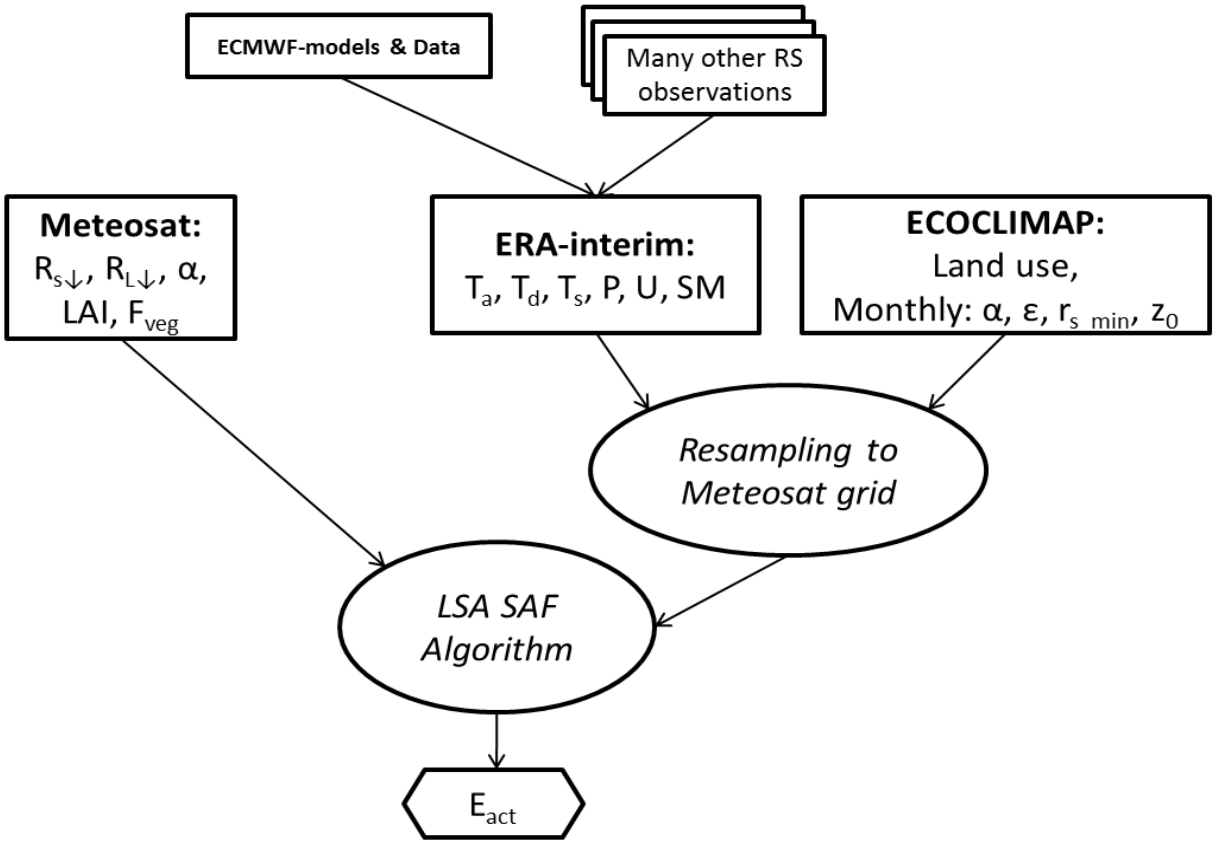

Figure 2-1 LSA SAF data sources. Based on Hurkmans and Klopstra (2015)

2.1.2 Theory and algorithm

In the LSA SAF algorithm, each pixel is split up into (a maximum of four) tiles, each tile representing a different type of soil surface. At tile level, the LSA SAF evaporation algorithm aims to compute the energy balance terms by solving (LSA SAF, 2010)

$$R_{n,i} - H_i - LE_i - G_i = 0 \tag{2-1}$$

Where $R_{n,i}$, H_i, LE_i and G_i are the fluxes (net radiation, sensible heat, latent heat and ground heat) in the tile. The estimate of net radiation is given by:

$$R_n = (1-\alpha)\,R_{s\downarrow} + \varepsilon\left(R_{L\downarrow} - \sigma T_{sk,i}^4\right) \tag{2-2}$$

Where α is the surface albedo, $R_{s\downarrow}$ is the incoming shortwave radiation, ε is the surface emissivity, $R_{L\downarrow}$ is the incoming longwave radiation, σ is the Stephen-Boltzmann constant and $T_{sk,i}$ is the skin temperature. The heat flux is estimated by:

$$G_i = B_i R_{n,i} \tag{2-3}$$

Where B is a fraction of the net radiation, and calculated as a function of the Leaf Area Index (LAI) via the Modified Soil Adjusted Vegetation Index (MSAV).

The latent heat flux is calculated using:

$$LE_i = \frac{L_v \rho_a}{r_{a,i} + r_{c,i}} \left[q_{\text{sat}} \left(T_{sk,i} \right) - q_a(T_a) \right] \tag{2-4}$$

Where L_v is the latent heat of vaporization, ρ_a is the air density, $r_{a,i}$ the aerodynamic resistance, q_a the specific humidity and q_{sat} the specific humidity at saturation. The aerodynamic resistance is based on the stability of the atmosphere, via the Obukhov length and friction velocity, as well as the sensible heat and momentum stability functions (LSA SAF, 2010). The canopy resistance r_c is calculated with:

$$r_c = \frac{r_{s,min}}{\text{LAI}} f_1 \left(R_{s\downarrow} \right) f_2 \left(\theta \right) f_3(D_a) \tag{2-5}$$

Where $r_{s,min}$ is the minimum stomatal resistance, and f_1, f_2 and f_3 the Jarvis functions related to transpiration stresses. The first Jarvis function is related to the incoming solar radiation required for photosynthesis, where:

$$f_1 \left(R_{s\downarrow} \right)^{-1} = \min \left(1, \frac{bR_{s\downarrow} + c}{a \left(bR_{s\downarrow} + 1 \right)} \right) \tag{2-6}$$

In which a, b and c are empirical constants. The Jarvis function for water stress is;

$$f_2 \left(\theta \right)^{-1} = \frac{\theta - \theta_{\text{pwp}}}{\theta_{\text{cap}} - \theta_{\text{pwp}}} \tag{2-7}$$

Where θ is the average soil water content in the root-zone. θ_{pwp} is the permanent wilting point, and θ_{cap} is the field capacity. The last Jarvis function is related to the vapour pressure deficit in the air (D_a):

$$f_3 \left(D_a \right)^{-1} = exp(-g_D D_a) \tag{2-8}$$

Where g_D is an empirical constant.

To then calculate the latent and sensible heat flux requires iteration, as the variables (H, LE, T_{sk}, r_{ai}, and u^*) are interdependent. The iterations are stopped when the difference per iteration is deemed small enough. The global pixel value is then obtained through weighted averaging of the tiles.

2.2 Site descriptions

Multiple locations were studied. The two in the Netherlands, the Cabauw polder and the Hupsel Brook, have a large amount of data and background information available due to the large amount of studies done over the years. In Spain two catchments are studied without having detailed knowledge of them due a lack of data.

2.2.1 Cabauw polder

The Cabauw polder is located in the west of the Netherlands, between Utrecht and Rotterdam (Figure 2-2). It is located 1km from the Lek river. The polder does not have large elevation differences, and is well drained by drainage ditches about 30m apart, combined with drainage pipes. Preferential flow paths due to animal activity and gullies also occurs (Brauer et al., 2014b).

The polder has been used by the KNMI (Royal Dutch Meteorological Institution) for meteorological measurements for over 40 years. In recent times groundwater and soil moisture measurements have also been done, along with discharge measurements.

Actual evaporation data (measured using eddy covariance) is freely available since 2001 (Cesar Consortium, 2016). Also available is local precipitation and Makkink reference evaporation. Discharge measurements are available between 2007 and 2011. Seepage data is less detailed, and the water balance was studied to determine the possible seepage (see Appendix B).

Figure 2-2 Study site locations in the Netherlands (blue: Cabauw, red: Hupsel Brook)

2.2.2 Hupsel Brook catchment

The Hupsel Brook catchment lies in the east of the Netherlands (Figure 3). It has been extensively used for hydrological research since the 1970s, as the soil consists of a layer of loamy sand (0.2 to 10m) on top of an impermeable clay layer (Brauer et al., 2014b). This allows for easily closing the water balance, and tracking transport of solutes through the catchment. The elevation in the catchment ranges from 22 to 36 mNAP.

In the area the main land use is agriculture, and the land cover is roughly 45% corn, 50% grass and 5% forest (see Appendix A).

The fields are drained using both ditches and drainage pipes, and it is estimated that 25 to 50% of the measured discharge has been discharged through those drainage pipes (van der Velde, 2011).

During very dry years it is possible that farmers irrigate their land using sprinkling systems. As there is no deeper aquifer all the water will have to be extracted from the unconfined aquifer. This means that the water balance of the catchment will not have an extra (unknown) term. Sprinkling

however would avoid water stress in crops, and lower the groundwater table. The effect would not be noticeable when using actual evaporation data, but might mean that models using Makkink evaporation (without taking sprinkling into account) will differ from groundwater and evaporation measurements.

While the Hupsel Brook has been used for measurements since the 1970s, the focus shifted to water quality in the 1980s and no series of actual evaporation measurements is available since. The local KNMI weather station does the regular measurements (precipitation and reference evaporation being the relevant measurements).

The only available actual evaporation measurements available are from the dry summer of 1976, where the sensible heat flux was determined using the similarity model of Monin and Obukhov (Stricker and Brutsaert, 1978). The latent heat flux was then estimated by taking the remaining energy in the energy balance.

2.2.3 Water Board Hoogheemraadschap De Stichtse Rijnlanden (HDSR)

To use in this study, the Water Board Hoogheemraadschap De Stichtse Rijnlanden (HDSR) provided the SIMGRO model of their entire area (Figure 2-3), which is located in Utrecht, in the centre of the Netherlands. The area is varied, has peat polders in the west, and has sand hills in the east. In the model the rivers, canals and wells are incorporated, along with all the land use types and elevations.

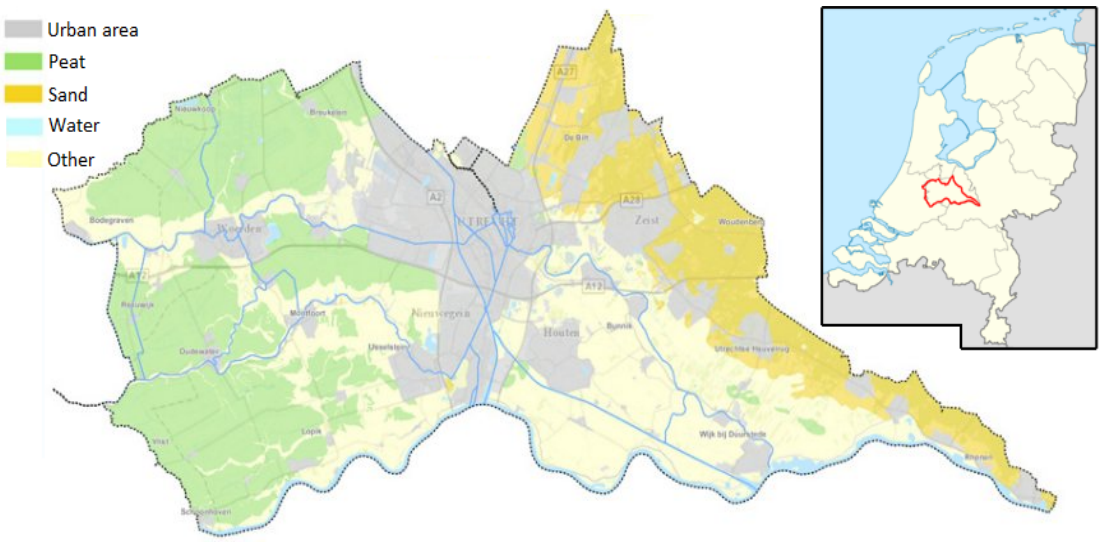

Figure 2-3 Area of the water board Stichtse Rijnlanden, within the Netherlands (Waterschap Online, 2016)

2.2.4 Spanish Catchments

As water stress in the Netherlands is rare and big droughts have not occurred since the start of the LSA SAF measurements, some dry areas will be studied. Due to the availability of a large number of stream flow measurements, Spain was chosen. The Spanish Ministry of Agriculture, Food and Environment has made a huge public database of discharge measurements available online (Ministerio de Agricultura Alimentación y Medio Ambiente, 2013). To select suitable rivers, the following criteria were used:

- Close proximity to a meteorological station
- Natural flow; no dams or reservoirs, or large scale irrigation
- Uniform landscape

The following two rivers were selected:

Ubierna river

The Ubierna catchment is located in the province of Burgos in the north of Spain, situated 20km north of the meteorological station of the city of Burgos at the southern slopes of the Cantabrian mountains (Figure 2-4). The terrain consists of gentle slopes, and is mainly used for rain fed agriculture. The catchment has an area of 288.4km^2, and discharge is measured using a stage-discharge relationship in a natural stream without fixed structure. This makes the discharge measurement quite unreliable.

Ulzama river

The Ulzama catchment is located in the autonomous community of Navarra, in the north of Spain and close to the Pyrenees (Figure 2-4). The terrain consists of forested hills and agriculture in the valleys. The catchment has an area of 231km^2, and the discharge measurements are done using a fixed concrete structure without a low flow channel. The amount of dense forest, and other green vegetation during summers seems to indicate that water stress is relatively low. The closest meteorological station is in Pamplona, about 15km from the catchment.

Figure 2-4 Locations of the catchments in Spain. Blue: Ubierna catchment, Red: Ulzama catchment

2.3 Model descriptions

Three different model structures are used in the study; WALRUS, SIMGRO, and FLEX. Each of them has a certain set of parameters which can be calibrated with.

The model calibration will be done using a Monte Carlo analysis (Smith and Hebbert, 1979). In the analysis a set of values for the calibration parameters is randomly generated within parameter bounds. The model will run each set of parameters for a calibration period, and the performance of the run will be evaluated using an objective function by comparing the modelled discharge to the observed discharge. The parameter set with the best performance will be seen as the optimal run.

To then evaluate the real performance of the model, the second time period is the validation period. The optimal parameter set will be used in a model run for the validation period. This will provide the final performance.

As objective function, the Nash-Sutcliffe model efficiency was chosen because of its common use in

hydrology (Nash and Sutcliffe, 1970)

$$NS = 1 - \frac{\sum \left(Q_{\text{obs}} - Q_{\text{mod}}\right)^2}{\sum \left(Q_{\text{obs}} - Q_{\text{obs}}\right)^2} \tag{2-9}$$

Where Q_{obs} is the observed discharge and Q_{mod} the modelled discharge (mm/d). The highest efficiency possible is 1, where the modelled discharge is exactly equal to the observed discharge. When the efficiency is 0, the modelled discharge performs as well as the mean of the observed discharge would.

As the Nash-Sutcliffe efficiency focusses on high flowrates, a modified version is possible. This is the logarithmic Nash-Sutcliffe efficiency, where the logarithm (base 10) of the discharge is used instead:

$$NS_{\log} = 1 - \frac{\sum \left(log(Q_{\text{obs}}) - log(Q_{\text{mod}})\right)^2}{\sum \left(log(Q_{\text{obs}}) - log(Q_{\text{obs}})\right)^2} \tag{2-10}$$

This objective function focusses on the baseflow, and can be used when getting the baseflow right is deemed more important than the peaks (Krause and Boyle, 2005).

To give the models the freedom to properly close the water balance when imposing actual evaporation (i.e. to make $\Delta S = 0$ on a multi-year time scale), an extra parameter is added. This is the evaporation factor (E_{factor}). The actual evaporation is multiplied by this factor to get the evaporation used by the model. The factor is added as a calibration parameter. The need for this factor arises from uncertainties in the measurements, mainly the accuracy of the actual evaporation, but also the accuracy of the measured discharge and precipitation. When a model uses potential evaporation the calibration can partially correct for this as it has a degree of freedom in the evaporation reduction, while that is not the case with actual evaporation. Similarly a factor for the rainfall and discharge is also possible, when the evaporation data is deemed to be more accurate than the precipitation or discharge data.

2.3.1 WALRUS

WALRUS is short for WAgeningen Lowland RUnoff Simulator, a conceptual rainfall-runoff model made specifically for simulating lowland catchments (Brauer et al., 2014a). It is developed by Claudia Brauer (Wageningen UR), and is programmed in the 'R' language, with the model code available online under the GNU General Public License (free, open source).

In this study WALRUS was chosen due to it being a simple conceptual and easy to modify model, and because it has been recently applied on the Hupsel Brook and Cabauw catchments in an extensive study (Brauer et al., 2014b).

In WALRUS multiple reservoirs and fluxes are modelled. The reservoirs are the soil water, the surface water and quickflow reservoirs (Figure 7). Precipitation enters the model (P), is split over open water (P_S) and over land, and is then divided over the soil water (P_V) and quickflow reservoirs (P_G) according to a soil wetness index (W).:

$$W(d_V) = cos(\frac{max(min(d_V, c_W), 0)\pi}{c_W})\frac{1}{2} + \frac{1}{2} \tag{2-11}$$

$$P_V = P(1-W)a_G \tag{2-12}$$

$$P_Q = PWa_G \tag{2-13}$$

Where a_G is the fraction of the catchment covered by land. Interception is not included in WALRUS, and should be added in the form of pre-processing the precipitation and evaporation data if including it is deemed necessary (Brauer et al., 2014a).

Water evaporates from the surface water and soil water. The rate from surface water (E_s) is always equal to potential evaporation. The evaporation rate from the soil (E_v) is the potential evaporation (E_{pot}) multiplied by the evaporation reduction factor (γ), which depends on the soil storage deficit (d_V).

$$E_v = E_{\text{pot}}\gamma \tag{2-14}$$

This leads to the evaporation reduction factor being described as:

$$\gamma = \frac{1-\exp\left(\zeta_1\left(d_v-\zeta_2\right)\right)}{1+\exp\left(\zeta_1\left(d_v-\zeta_2\right)\right)}\frac{1}{2}+\frac{1}{2} \tag{2-15}$$

Where ζ_1 controls the curvature (-) and ζ_2 controls the translation (mm) of the reduction function. By default the parameters are $\zeta_1 = 0.02$ and $\zeta_2 = 400$, these are based on an empirical relationship derived from measurements (Brauer, Teuling, et al., 2014). To illustrate the function, the relationship between moisture deficit and evaporation reduction is shown in Figure 2-5.

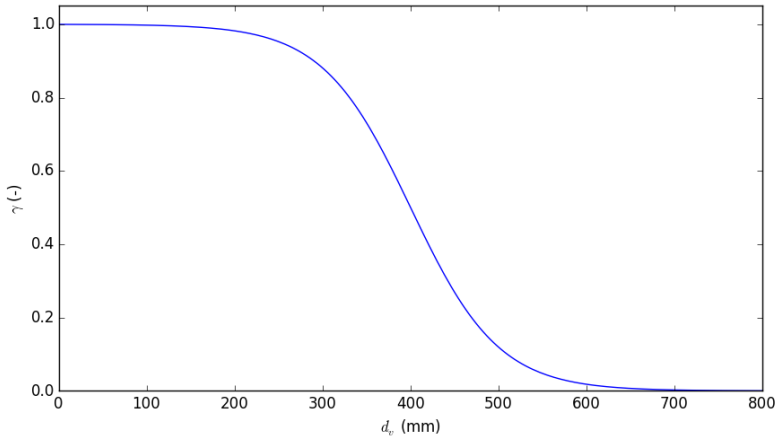

Figure 2-5 Default evaporation reduction function in WALRUS

The unsaturated zone is modelled using the groundwater depth (d_G), and the soil storage deficit. The storage deficit changes due to rainfall the land, evaporation, and from interaction with the surface water (f_{GS}) and seepage (f_{XG}). The change is also related to the groundwater reservoir area fraction (a_G):

$$\frac{\mathrm{d}\ d_V}{\mathrm{dt}} = -\frac{f_{\text{XG}} + P_V - E_V - f_{\text{GS}}}{a_G} \tag{2-16}$$

The ground water area fraction is the fraction of the catchment which is not open water. The groundwater depth is related to the storage deficit and equilibrium storage deficit:

$$\frac{\mathrm{d}\, d_G}{\mathrm{dt}} = \frac{d_V - d_{V,eq}}{C_V} \tag{2-17}$$

Where C_V is the vadose zone relaxation time. The equilibrium storage deficit is described as:

$$d_{V,eq} = \theta_S \left(d_G - \frac{d_G^{1-\frac{1}{b}}}{\left(1-\frac{1}{b}\right)\psi_{\mathrm{ae}}^{-\frac{1}{b}}} - \frac{\psi_{\mathrm{ae}}}{1-b} \right) \tag{2-18}$$

Where θ_S is the moisture content of the soil at saturation, ψ_{ae} is the air entry pressure and b is the pore size distribution parameter. These soil parameters can be determined from local measurements.

Flow from the groundwater to the surface water is modelled like a linear reservoir, governed by the height difference between the groundwater and surface water and the response factor C_G. The quickflow reservoir drains like a simple linear reservoir with response factor C_Q. The discharge from the surface water (Q) is modelled using a stage-discharge relation, which can be put into the model.

Lastly, seepage from (or infiltration into) deeper groundwater has to be put into the model using a fixed time series, and is not dependent on water levels within the model. The actual evaporation will be imposed according to the method described in Appendix D.

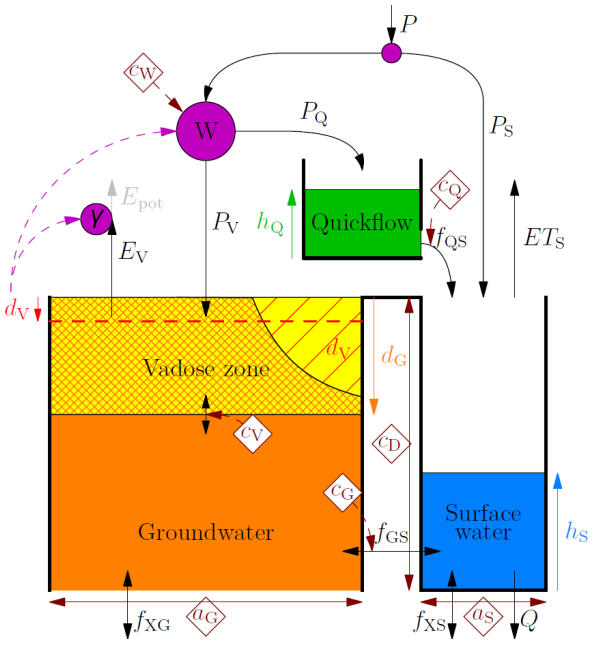

Figure 2-6 WALRUS model structure (Brauer et al., 2014a)

2.3.2 SIMGRO

SIMGRO is an integrated model consisting of multiple modules; a SVAT module (Soil-vegetation-atmosphere transfer model) for the plant-atmosphere interactions and soil water, a simplified surface water model, a drainage package, and a coupling to MODFLOW to model groundwater (van Walsum et al., 2010).

In SIMGRO the SVAT units are vertical columns; only interacting with each other via the connections to surface water and groundwater and not laterally with other SVAT units. The unsaturated zone is modelled using the Richards equation. The most important parts included in MetaSWAP (the SVAT module) are;

- Precipitation
- Interception
- Surface runoff
- Evaporation and transpiration
- Capillary rise and percolation governed by the Richards equation

The precipitation used is raw input into the model. Interception and transpiration are mainly governed by the land use type; ranging from crop types to urban area. Each crop type has its own values for the parameters (like leaf area index, root zone depth, evaporation crop factors).

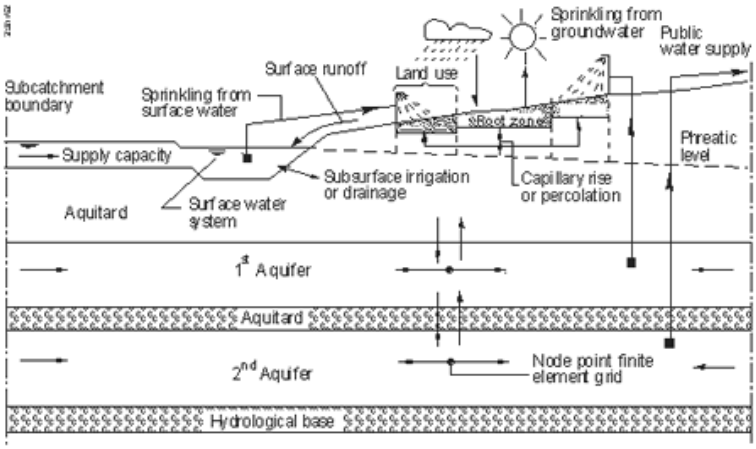

Figure 2-7 SIMGRO model processes overview (Veldhuizen, 2016)

In SIMGRO evaporation consists of multiple parts. Transpiration by plants, interception evaporation, bare soil evaporation, ponding evaporation and evaporation of sprinkling water. In the studied models sprinkling is not included, so it will not be looked at further. All forms of evaporation calculated in SIMGRO are based on factors applied to the reference evapotranspiration, which has to be entered into the model as input data (either Penman-Monteith or Makkink reference evaporation, in this study Makkink has been used).

Potential transpiration (T_p) is calculated by applying the crop coefficient (K_{cb}) on the reference crop evapotranspiration (E_0). The crop coefficient depends on the crop and time of year.

$$T_p = K_{cb} E_0 \tag{2-19}$$

This potential transpiration is then modified for evaporation reduction using a Feddes reduction function (Feddes et al., 1978), which is dependent on the pressure head in the soil (Figure 2-8). Application of the reduction coefficient then leads to actual transpiration (T_a):

$$T_a = \alpha_E T_p \tag{2-20}$$

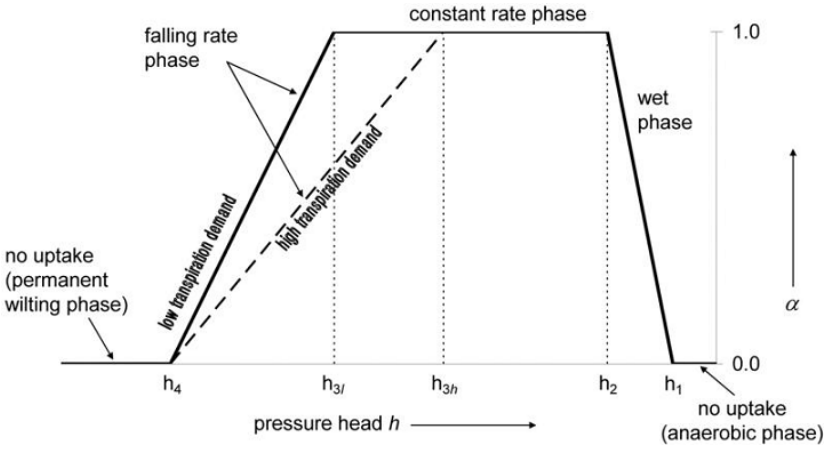

Figure 2-8 Feddes evaporation reduction function (de Jong van Lier et al., 2008)

Precipitation which is intercepted by plants is modelled as a bucket in SIMGRO. From this bucket water evaporates at a rate of a factor multiplied by the reference evaporation. Interception evaporation suppresses the transpiration, due to the lower resistance of the interception water compared to the water evaporation from the stomata. As long as the process is active, no transpiration takes place. The rate of interception evaporation (E_{ic}) is related to the reference evapotranspiration times a factor (K_i), which is 1.15 by default:.

$$E_{ic} = K_i E_0 \tag{2-21}$$

Evaporation from ponding is modelled with a bucket model, which evaporates at the rate of a factor (K_{pond}) times the reference evapotranspiration, while there is water on the surface.

$$E_{pond} = K_{pond} E_0 \tag{2-22}$$

In SIMGRO bare soil evaporation is calculated separately from the transpiration, and is related to the cumulative values of actual and potential evaporation since the start of the drying period. In practice, soil evaporation in SIMGRO is about 0.1 to 0.2 times the reference evapotranspiration in summer, and around 0.3 times E_0 in winter, depending on the land cover, precipitation, etc.

The actual evaporation is the sum of all the different forms of evaporation. This is the evaporation which will be compared to actual evaporation measured by eddy covariance and LSA SAF.

Besides the large SIMGRO-HDSR model, a single cell SIMGRO model of Cabauw has also been made to make the analysis easier, and calibration feasible. The bottom boundary in Modflow is set as a hydraulic head time series. The model has only one MetaSWAP unit for the unsaturated zone, representing the catchment.

The actual evaporation will be imposed on WALRUS according to the method described in Appendix C.

2.3.3 FLEX

The conceptual model used is based on the lumped FLEX model (Gao et al., 2014), however as only areas with uniform landscapes will be studied, no different topographical units are added. The model consists of four reservoirs; interception (S_i), the unsaturated zone (S_U), quickflow (S_f) and

baseflow (S_s) (Figure 10). Precipitation (P) enters through the interception reservoir, which has a certain depth ($I_{\max}$). Any throughfall (P_{tf}) will spill over into the other reservoirs.

Part of the throughfall will runoff to the groundwater. This is governed by the equations:

$$R_u = C_r P_{\text{tf}} \tag{2-23}$$

$$C_r = \frac{1}{1 + e^{\frac{-S_U/S_{U,max}+0.5}{\delta}}} \tag{2-24}$$

Where R_u is the runoff to the quickflow and baseflow reservoirs, C_r is the runoff coefficient, $S_{u,max}$ is the maximum moisture storage in the root zone, and δ is a parameter describing the spatial heterogeneity.

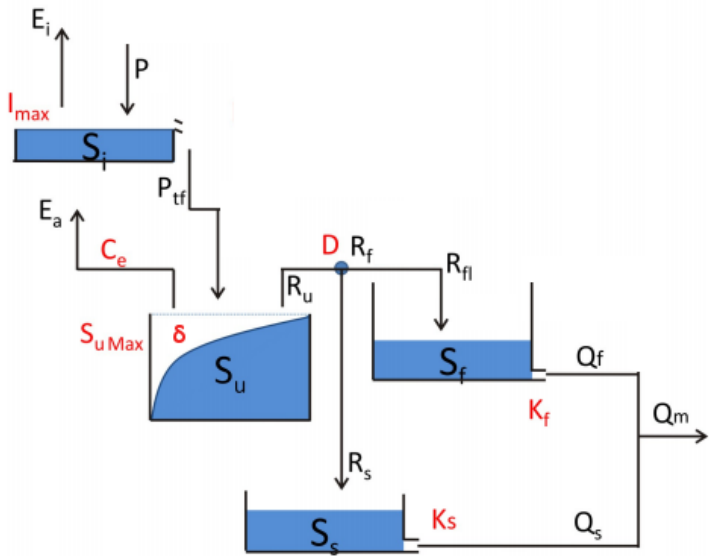

Figure 2-9 FLEX model structure. Based on Gao et al. (2014)

The runoff is split between the baseflow and quickflow reservoirs using the divider D. These reservoirs are linear reservoirs, with parameters K_f and K_s. The outflow (Q_f and Q_s) makes up the modelled discharge (Q_m).

Evaporation in the model is first extracted from the interception reservoir, at the rate of actual or potential evaporation. What is left will then be applied to the unsaturated reservoir. In the case of potential evaporation it is reduced using the following equation:

$$E_a = (E_{\text{pot}} - E_i) \min\left(\frac{S_U}{C_e S_{U,max}},\ 1\right) \tag{2-25}$$

Where C_e is the fraction above which no reduction takes place.

The procedure to set up the models will be to first acquire the discharge data and basin area, along with the LSA SAF evaporation and station data. Then the model will be calibrated using the free parameters, with as objective function the log-Nash-Sutcliffe efficiency of the discharge.

The focus will be on the baseflow; as there is a high uncertainty in rainfall peaks, the peaks will often not be modelled well due to heterogeneity, while the baseflow can be. After this the model will be run on the verification period and the performance assessed.

3 Comparing the LSA SAF product

To verify the LSA SAF evaporation locally, it can be compared to eddy covariance measurements at Cabauw. Other reliable actual evaporation measurements are not openly available within the Netherlands or in the studied areas in Spain. A validation study has been done for the LSA SAF product, comparing it to a number of eddy covariance stations within Europe. It shows that the product performs well when looking at the correlation with measurements, although the bias can be quite significant (Hu et al., 2015).

When comparing the LSA SAF actual evaporation against local eddy covariance measurements at Cabauw (Figure 3-1), the correlation is very strong but the eddy covariance based data gives higher estimates than the LSA SAF evaporation. It is important to note that while LSA SAF will never give negative evaporation rates, eddy covariance can. A negative evaporation rate can mean that dew is being formed at the ground surface. The general overestimation of the eddy covariance system can have multiple causes; the LSA SAF measured area is different from the eddy covariance footprint, the way of correcting the eddy covariance data is prone to slight overestimations, and the input data and assumptions of the LSA SAF algorithm do not correspond completely with the local conditions.

The LSA SAF data has also been split for cloud cover, as the Meteosat satellite cannot make surface observations at those time, and the LSA SAF model has to use data from models, extrapolation, and other sources. The correlation for clear skies is slightly different than on cloudy days, but this is also influenced by the local situation during clear skies; more dew formation will occur due to the lower surface temperature at night (represented by the negative evaporation values of the eddy covariance data). The consistent difference between the cloudy and clear sky observations are due to a difference in input data source for the different conditions. A different formulation for the incoming shortwave radiation is used, along with a different source for the albedo (ECOCLIMAP instead of direct Meteosat-10 observations).

Table 3-1 Statistics of the regression between EC and LSA SAF, split between clear and cloudy days

	Slope	Intercept	R^2
Cloudy days	0.785	-0.044	0.898
Clear days	0.816	0.246	0.963

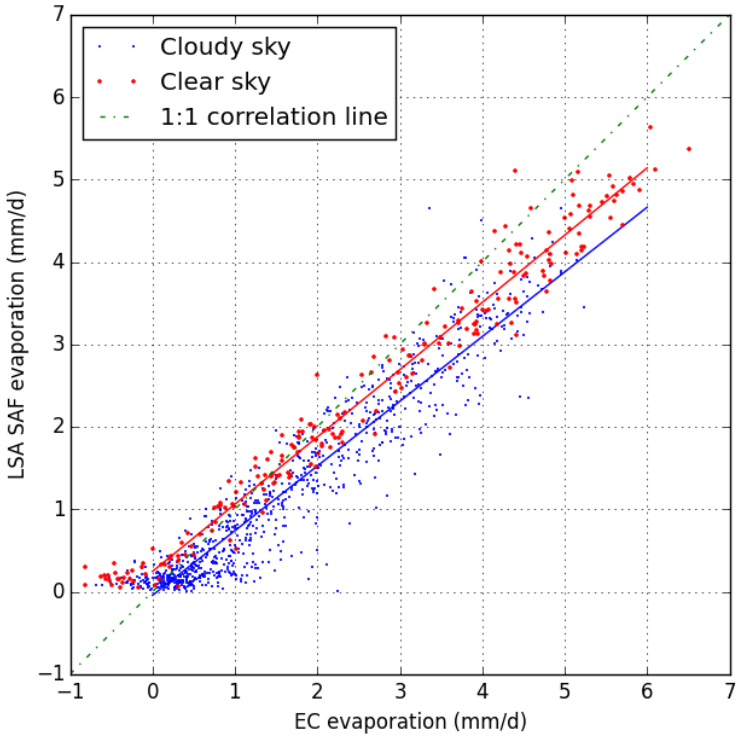

Figure 3-1 Correlation between eddy covariance and LSA SAF. Hourly data from 2011 to 2013. Red: Clear sky days. Blue: Cloudy days.

When looking at the evaporation rates during the years (Figure 3-2), it shows that the difference between the eddy covariance and the LSA SAF actual evaporation is not uniform. During winter the eddy covariance estimate is slightly higher, but very variable (and at times unrealistic; for example a negative evaporation rate for multiple days). In summer eddy covariance gives a higher estimate, but this difference is not constant.

As shown in Figure 3-3, the ratio between the eddy covariance and LSA SAF evaporation varies during the year. However, during winter (when relative errors are largest) evaporation is barely significant. During summer the ratio varies between 1.0 and 1.2. The absolute difference is on average 0.2mm/d, but varies a lot.

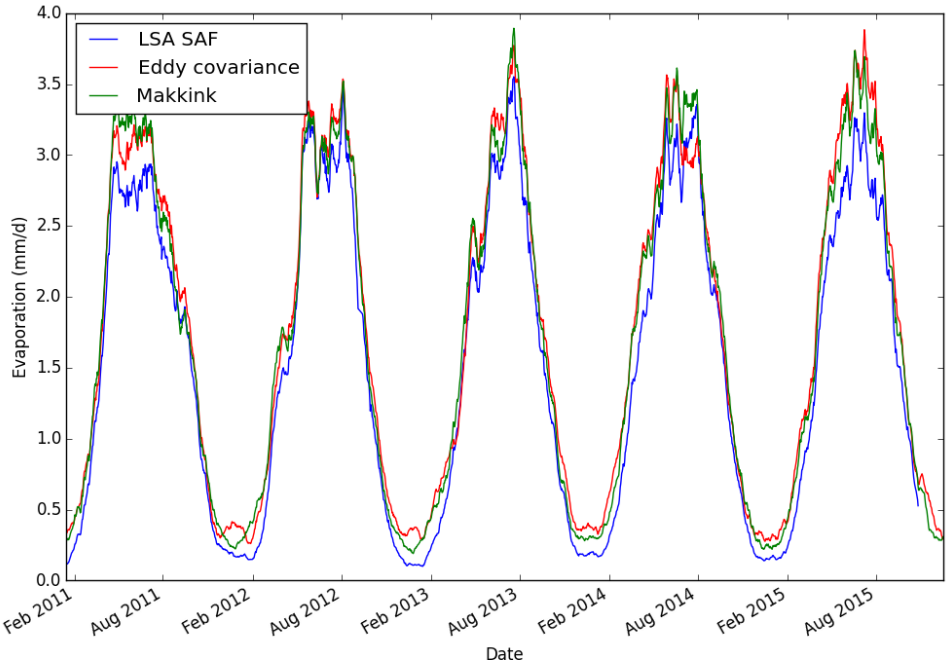

Figure 3-2 30 day moving average of the evaporation rates at Cabauw. Data from eddy covariance and LSA SAF and Makkink evaporation.

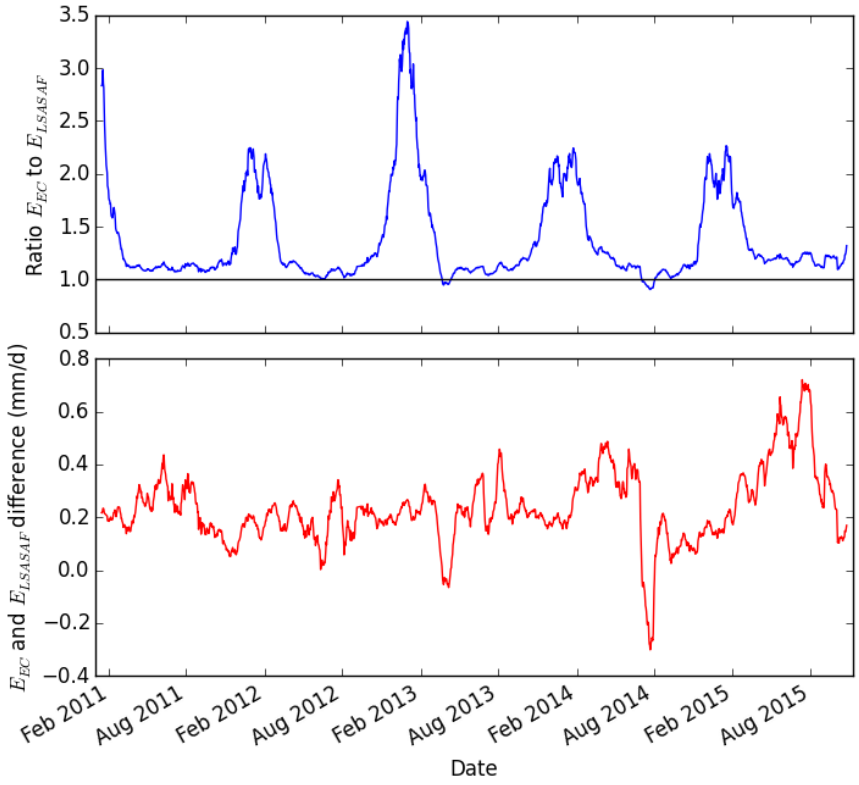

Figure 3-3 Ratio and difference between the eddy covariance and LSA SAF actual evaporation estimates, 30 day moving average

4 Results and discussion of imposing actual evaporation on different models

4.1 WALRUS

4.1.1 Comparison at Cabauw

The WALRUS model of Cabauw was calibrated on data from 2007/05/23 to 2009/01/01, using either Makkink evaporation or actual evaporation. For the calibration a Monte Carlo analysis was used, using 4000 runs. The calibration parameters were C_W, C_V, C_G, C_Q and the E_{factor}. As the LSA SAF product is only available from 2011, the eddy covariance actual evaporation is used. It's assumed, based on Figure 3-1, that eddy covariance actual evaporation is similar enough to the LSA SAF evaporation, except for a constant correction factor on the LSA SAF evaporation.

In Figure 4-1 the optimal runs (with the highest Nash-Sutcliffe efficiency) are shown, along with the observed discharge. The timing and magnitude of the peaks are generally well modelled, although the baseflow during the winter of 2009/2010 is estimated too high.

The difference between the Makkink evaporation and the actual evaporation calibrated discharges is very small, and barely significant.

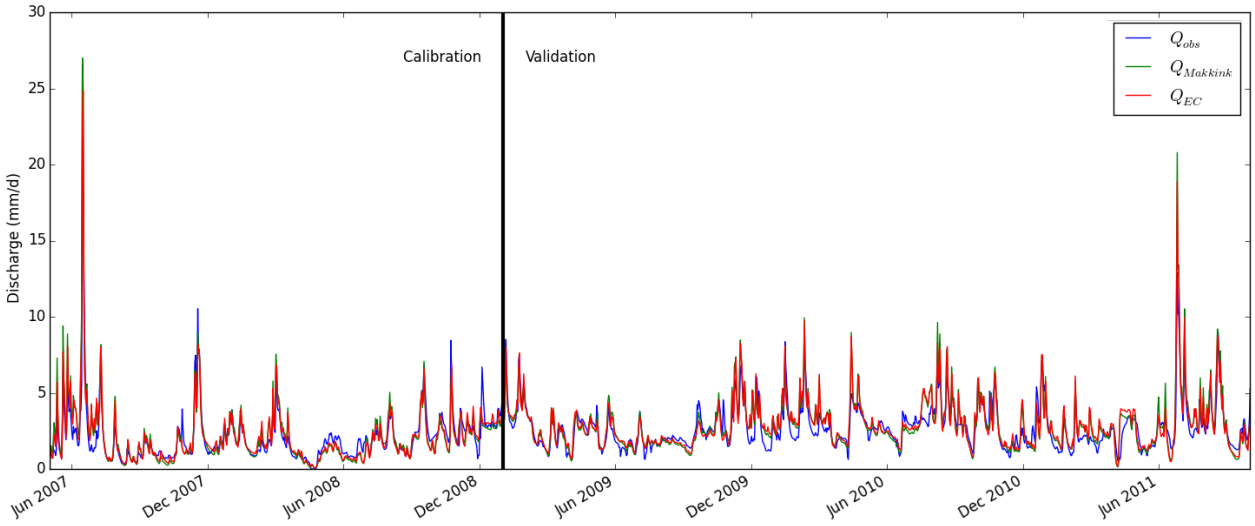

Figure 4-1 Discharge plots of the optimal runs of the Cabauw model. Using the $\mathbf{E}_{factor}$.

When looking at the model efficiencies during calibration, they are all in a very small range. The addition of the evaporation factor gives an insignificant improvement (Table 4-1).

Table 4-1 Nash-Sutcliffe efficiency of the calibration period, for Cabauw

Calibration	With $\mathbf{E}_{\text{factor}}$	No $\mathbf{E}_{\text{factor}}$
EC actual evaporation	0.854	0.851
Makkink potential evaporation	0.837	0.834

During the validation period the model using actual evaporation performs slightly better (Table 4-2). The differences between the models using the evaporation factor and not are insignificant.

Table 4-2 Nash-Sutcliffe efficiency of the validation period, for Cabauw

Validation	With $\mathbf{E}_{\text{factor}}$	No $\mathbf{E}_{\text{factor}}$
EC actual evaporation	0.693	0.689
Makkink potential evaporation	0.673	0.679

When analysing the sensitivity of the evaporation input, by looking at the evaporation factor, it shows that the precision of the actual evaporation is very important (Figure 4-2). There is a very clear peak around $E_{\text{factor}} = 1.00$. However, when looking at the Makkink evaporation model, this is much less clear. The reason for the optimum around the evaporation factor of 1.00 for the actual evaporation is probably because of the way that the seepage has been determined; this was done by closing the water balance using the precipitation, eddy covariance actual evaporation, and measured discharge. This leads to the water balance closing in the model when the evaporation factor is exactly 1.

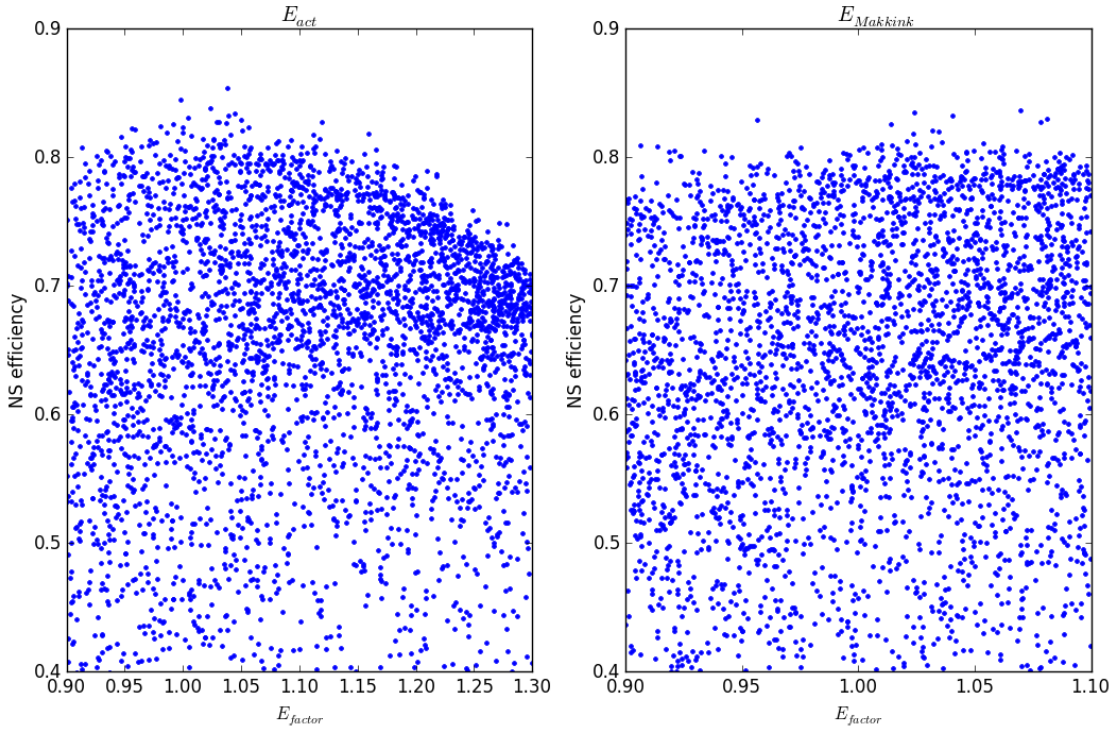

Figure 4-2 Sensitivity plot $\mathbf{E}_{factor}$ for the calibration of the Cabauw model

When comparing the different evaporation data throughout the year (Figure 4-3), it shows that there are just small differences, sometimes the Makkink evaporation is slightly higher, and sometimes eddy covariance gives higher results. Mainly in winter some differences appear, when the eddy covariance method gives negative evaporation rates. It also shows that in the model no water stress at all occurs.

When looking at the cumulative evaporation (Figure 4-4), there is also barely a difference. The Makkink evaporation is slightly lower in summers (10 to 20mm over the season) and slightly higher in winters (15 to 30mm over the season).

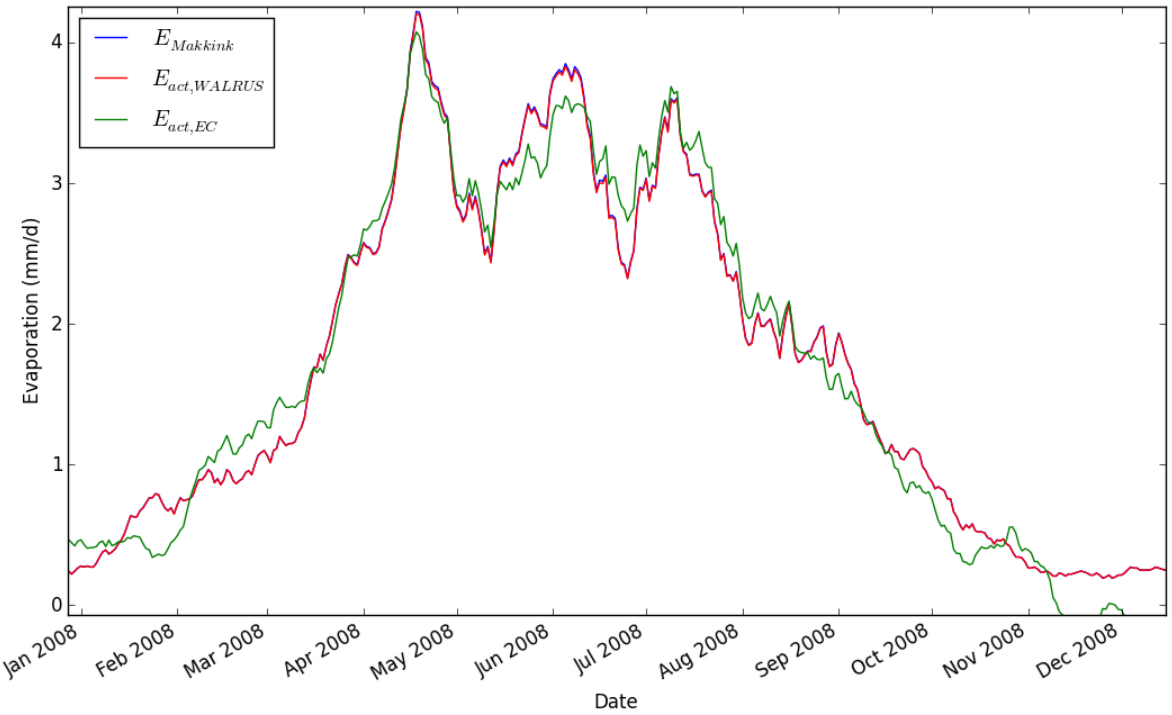

Figure 4-3 Evaporation comparison between the Makkink evaporation ($\mathbf{E}_{Makkink}$), reduced evaporation ($\mathbf{E_{act,\ WALUS}}$) and eddy covariance actual evaporation ($\mathbf{E_{act,\ EC}}$) at Cabauw. (Moving average of 14 days.)

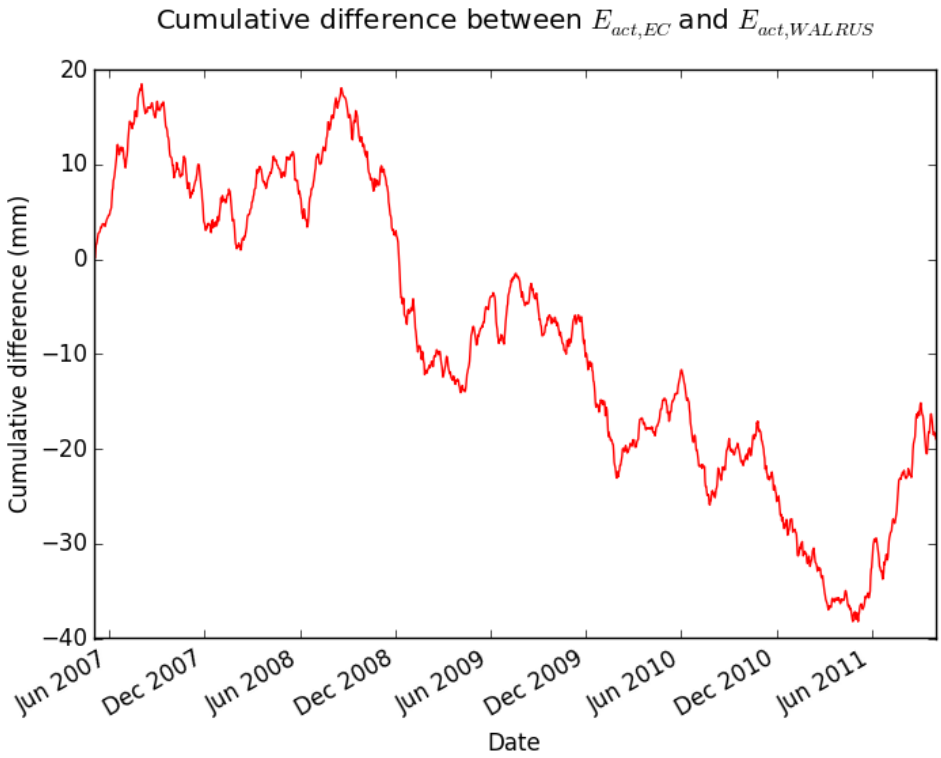

Figure 4-4 Cumulative difference between the eddy covariance evaporation, and the actual evaporation calculated using Makkink evaporation at Cabauw ($\sum(\mathbf{E_{act,EC}} - \mathbf{E_{act,WA:LRUS}})$)

4.1.2 Comparison at the Hupsel Brook

The WALRUS model of the Hupsel Brook was calibrated on data from 2011-01-01 to 2013-01-01, using either Makkink evaporation or LSA SAF actual evaporation. For the calibration a Monte Carlo analysis was used, using 2500 runs. The calibration parameters were C_W, C_V, C_G, C_Q and the E_{factor}.

To get the LSA SAF actual evaporation data for the catchment, the area average was calculated using a polygon of the catchment and the LSA SAF data raster. The size of the catchment (6.5km^2; about 2x3km) is much smaller than the size of the LSA SAF raster elements. Because of this the actual evaporation is not completely representative for the Hupsel Brook catchment as it also includes the surrounding landscape and towns. The general landscape around the catchment is quite similar in land use and geology, so it is assumed that the data is sufficiently representative to use on the small catchment.

When preparing the Makkink evaporation for the WALRUS model the following crop coefficients were used:

Table 4-3 Crop coefficients Hupsel Brook (De Bruin and Lablans, 1998)

	Jan	Feb	Mar	Apr	May	Jun	Jul	Aug	Sep	Oct	Nov	Dec
Grass	0.9	0.9	0.9	1.0	1.0	1.0	1.0	1.0	0.9	0.9	0.9	0.9
Maize	0.2	0.2	0.2	0.2	0.7	1.0	1.3	1.2	1.2	0.2	0.2	0.2
Forest	1.0	1.0	1.0	1.0	1.0	1.0	1.0	1.0	1.0	1.0	1.0	1.0
Catchment	0.60	0.60	0.60	0.65	0.87	1.00	1.13	1.09	1.04	0.60	0.60	0.60

As objective function for the calibration, the Nash-Sutcliffe efficiency was used. The calibration resulted in good NS efficiency values (Table 4-4), but when comparing the discharge data some problems can been seen (Figure 4-5). The high peaks are not modelled sufficiently, and are generally underestimated (with both evaporation inputs). Besides this, the base flow does not seem to be modelled well. As visible in spring of 2011, and around March 2012, the base flow is much too high and should fall quicker, or the quickflow is not modelled well enough. The timing of the peaks coincides very well with the observed data, and the first peaks after summer are also caught, albeit not at the right magnitude.

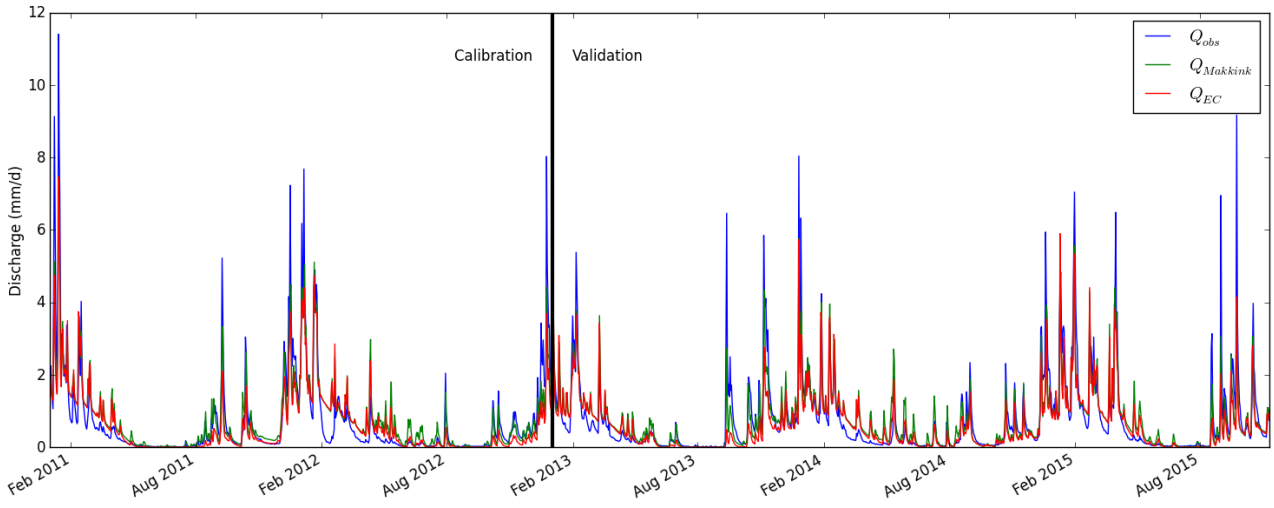

Figure 4-5 Calibration and validation period Hupsel Brook, with $\mathbf{E}_{factor}$ (More detailed plot is visible in Appendix G)

Table 4-4 Nash-Sutcliffe efficiency of the calibration period, for the Hupsel Brook

Calibration	With $\mathbf{E}_{\text{factor}}$	No $\mathbf{E}_{\text{factor}}$
LSA SAF actual evaporation	0.815	0.772
Makkink potential evaporation	0.802	0.787

The E_{factor} of the best runs were 0.909 for the actual evaporation, and 1.015 for the Makkink evaporation.

When looking at the validation period, the same general trend as in the calibration period is visible. Base flow is too high, and peaks are too low. While the Nash-Sutcliffe efficiencies were very similar during the calibration period, a bigger difference does occur when looking at the evaluation period (Table 4-5). The model using actual evaporation seems to slightly outperform the model using Makkink evaporation.

Table 4-5 Nash-Sutcliffe efficiency of the validation period, for the Hupsel Brook

Validation	With $\mathbf{E}_{\text{factor}}$	No $\mathbf{E}_{\text{factor}}$
LSA SAF actual evaporation	0.762	0.690
Makkink potential evaporation	0.733	0.724

Evaporation Sensitivity

For both the actual and the Makkink evaporation, the addition of a calibration factor on the evaporation improves the model performance, as would be expected. By plotting the sensitivity plot the effect can be more closely analysed (Figure 4-6). It shows that the addition of the factor will mainly improve the performance of the model using actual evaporation, while the effect on the model using Makkink evaporation will be much smaller, and does not show a clear optimum.

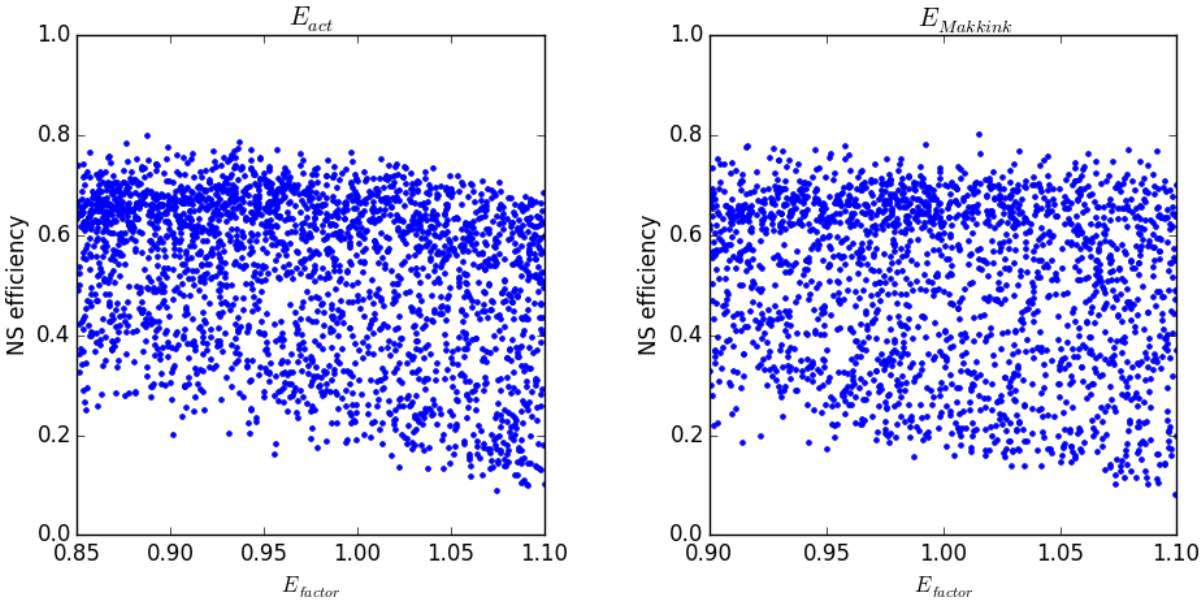

Figure 4-6 Sensitivity plot for the evaporation factor. Left: Actual evaporation, Right: Makkink evaporation

To compare the different evaporation data, the data was put through a moving average filter (of 14 days) to remove the short term peaks (Figure 4-7). It shows that, while overestimating, the LSA SAF actual evaporation does follow the trend of the model-reduced Makkink evaporation well, and

does seem to recognise the times where evaporation is limited by the water stress (July – September 2013).

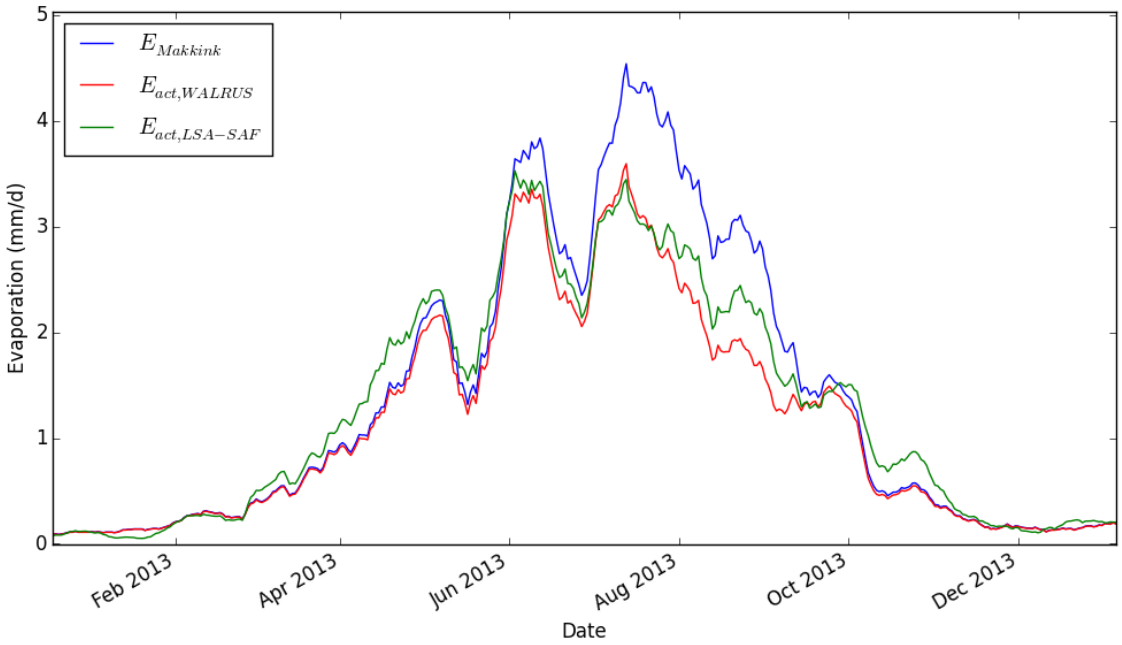

Figure 4-7 Evaporation comparison between the Makkink evaporation ($\mathbf{E}_{pot}$), model evaporation ($\mathbf{E_{act}}$, $\mathbf{WALUS}$) and LSA SAF actual evaporation ($\mathbf{E_{act}}$, $\mathbf{LSA-SAF}$) at the Hupsel Brook. (Moving average of 14 days.)

To make a more detailed comparison between the model-reduced evaporation and LSA SAF actual evaporation, the cumulative difference were calculated (Figure 4-8). Differences mainly build up during spring, where the LSA SAF evaporation exceeds the Makkink evaporation. When applying the calibrated evaporation factor however, the differences are much smaller and are negligible when averaged of a full year.

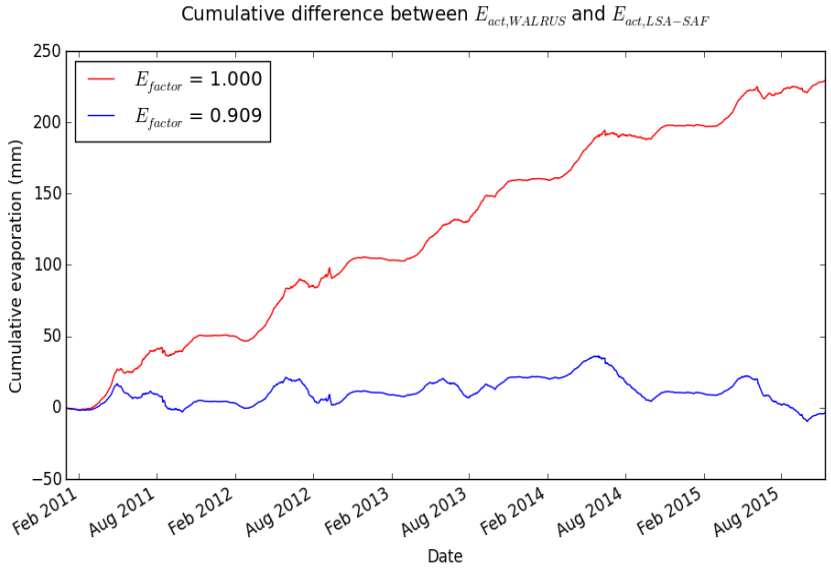

Figure 4-8 Cumulative difference between the actual evaporation calculated using Makkink evaporation, and the LSA SAF actual evaporation.

Instead of calibrating the factor, if sufficient data is available it can also be calculated. As the water balance has to close, the following equation should be valid on a larger time scale (such as a year):

$$P - Q - E_{\text{act}} E_{\text{factor}} = 0 \tag{4-1}$$

Using the sums of the input data (between 2011 and 2015) for the Hupsel, this leads to:

$$E_{\text{factor}} = \frac{\Sigma(P-Q)}{\Sigma(E_{\text{act}})} = 0.887 \tag{4-2}$$

This factor is in the centre of the optimum E_{factor} determined using the calibration (Figure 4-9), and shows that if closing the water balance is possible, the remote sensed actual evaporation can perform very well, and better than Makkink evaporation.

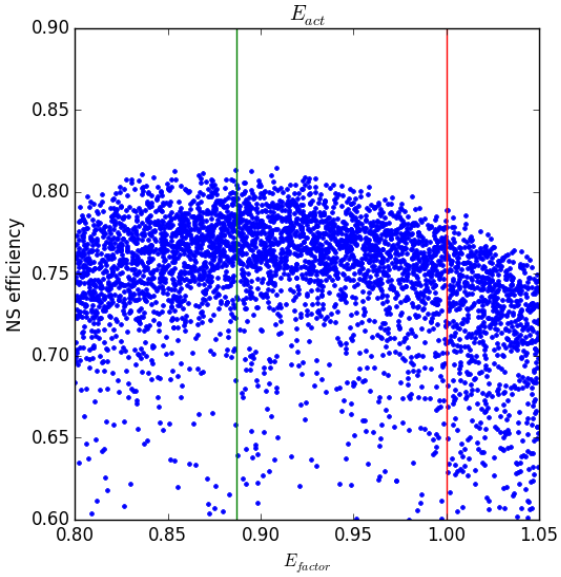

Figure 4-9 $\mathbf{E}_{factor}$ *efficiency plot, more extensive run. Green: water balance closure. Red:* $\mathbf{E}_{factor} = 1$

Improving the model performance

As the model performance lacks in certain aspects (heights of discharge peaks, baseflow), either the model parameters or model assumptions are not completely correct. One other problem in the Hupsel Brook is that by default, the WALRUS model does not model the groundwater difference over a year well (Figure 4-10). The variation from measurements over a year is nearly a meter, while it is half of that in the model.

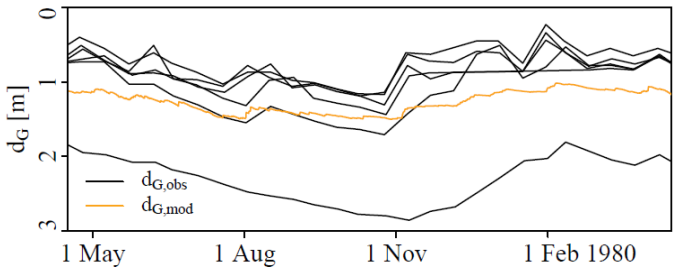

Figure 4-10 Groundwater observations and modelled in the Hupsel Brook (Brauer et al., 2014b)

From these observations, the storage parameters seem off. To improve this the soil moisture content at saturation (θ_S) was taken into the calibration, instead of getting it from the soil type. All other calibration parameters were also included in this calibration (as changing the θ_S will have a big influence on the performance). The evaporation factor was set to the found optimum (0.89), and the LSA SAF actual evaporation was used.

The Nash-Sutcliffe efficiency of the calibration was found to be 0.866. The efficiency of the validation period was 0.825. Both better than previously found. The optimum θ_S value was found to be 0.235 (Figure 4-11).

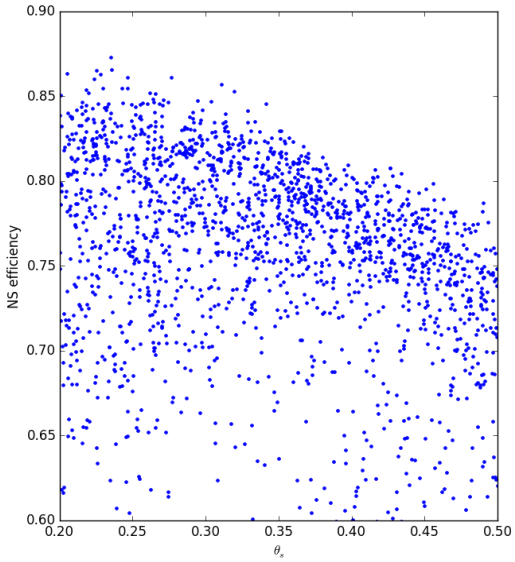

Figure 4-11 Efficiency plot of the θ_S calibration

When comparing the modelled discharge to the observed discharge, the baseflow modelling seems moderately better, and the height of peaks is modelled better. However, the low value of θ_S is completely unrealistic. This could show that the processes modelled in WALRUS do not approach reality well enough, or that the geology of the Hupsel Brook is too heterogeneous to be modelled as a single unit in WALRUS.

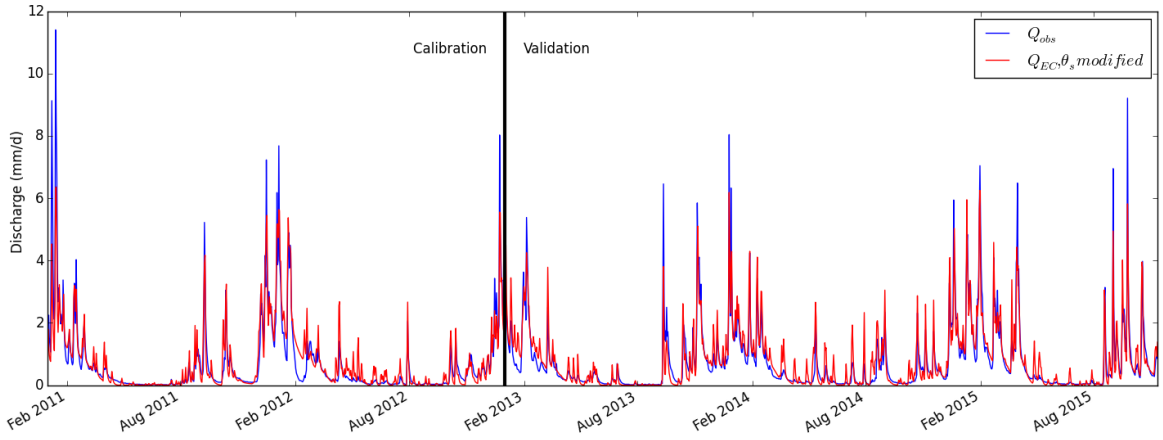

Figure 4-12 Observed and modelled discharge of the Hupsel Brook. The modelled discharge uses a modified θ_S. (More detailed plot is visible in Appendix G)

4.1.3 WALRUS Summary

The WALRUS model structure is flexible and easily adaptable, and thus very suitable for using actual evaporation data as input. It will still perform the way it is supposed to, without the need to trick the model intro working with actual evaporation. It can also be easily calibrated using just four calibration parameters, reducing the problem of equifinality.

However, at Cabauw actual evaporation data does not have much to add. In the studied period there was no period dry enough to cause water stress in the vegetation, and evaporation was always as high as the potential rate. In a location like Cabauw extreme weather is needed, or other irregular conditions, before water stress will lead to a lower evaporation. Besides this, the differences between the different evaporation methods are minimal enough to not make a difference when modelling the discharge. The WALRUS model was able to model discharge very well with eddy covariance as well as Makkink evaporation as input.

In the Hupsel Brook some water stress does occur, although there was no extremely dry year in the studied period. Because of this the differences between the LSA SAF and Makkink evaporation were small. When directly comparing the model performance with the different evaporation inputs, actual evaporation could improve the model, but only if the LSA SAF evaporation was corrected (by a fixed factor) to close the water balance.

4.2 SIMGRO

For SIMGRO two models of Cabauw are used. First is a model of the complete area of the Water Board Hoogheemraadschap Stichtse Rijnlanden (HDSR, encompassing 300,000 model cells), and the second one is a single cell model to make analysing what happens at the Cabauw polder easier.

The Cabauw polder has an inlet on one side, and an outlet on the other side (Bosveld, 2014). As such there is the extra boundary condition of the inflow. This inflow is variable, and depends on upstream conditions and control by the Water Board. The inflow is measured, but in SIMGRO this cannot be directly applied to the model. Only control conditions can be added. As such, the net discharge ($Q_{\text{net}} = Q_{\text{out}} - Q_{\text{in}}$) will be compared to the modelled discharge. The effect of this will mainly be visible in summer, when the inflow supplies water to the polder, leading to a negative net discharge.

4.2.1 SIMGRO-HDSR

In the HDSR model the cells corresponding to the Cabauw polder will be studied. This is due to the availability of local measurements, both on evaporation and groundwater, as well as discharge measurements. Other areas will not be studied, as there is a lack of local measurements to verify the model. As input into the model distributed rainfall and Makkink evaporation data is used.

When looking at Cabauw in the SIMGRO-HDSR model, it is quickly visible that several things are going wrong. A large evaporation reduction is taking place during summers (Figure 4-13), while this is most certainly not the case, as the eddy covariance measurements have shown. Even during mildly dry periods evaporation reduction due to water stress occurs in the model.

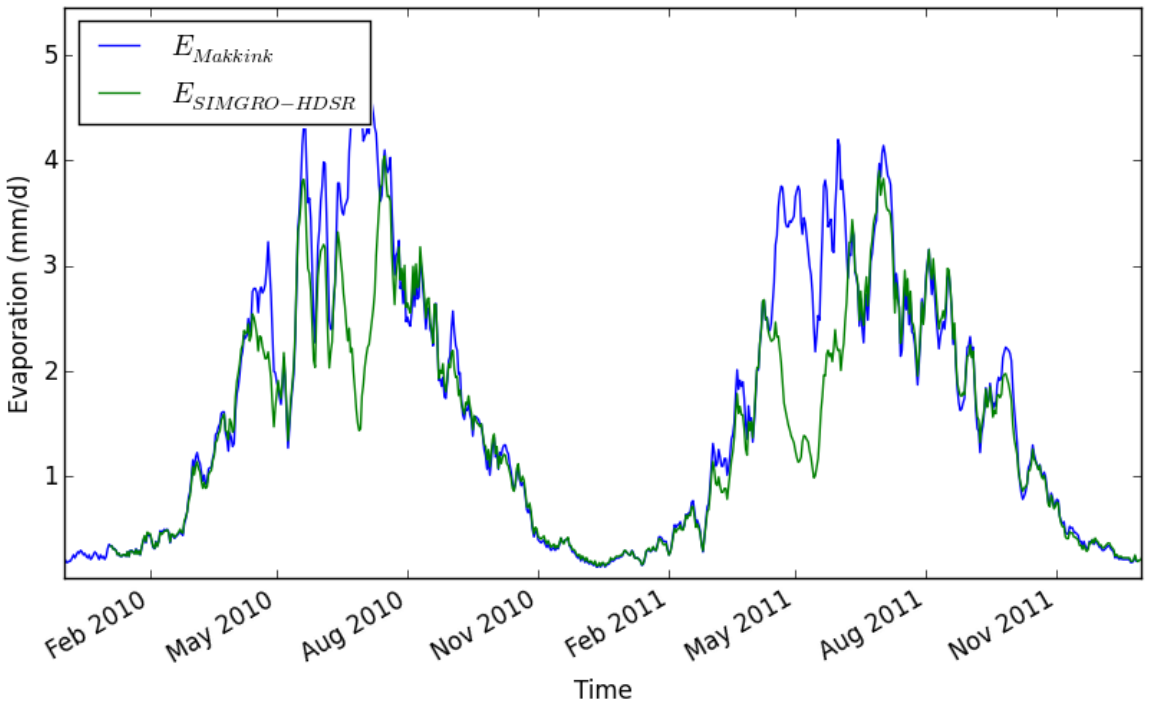

Figure 4-13 Makkink evaporation and model-reduced evaporation at Cabauw, 2010-2011. 7 day moving average.

Besides the differences in evaporation, the seepage is wrong. In the SIMGO-HDSR model a small infiltration into the deeper groundwater is modelled (Figure 4-14), while the opposite happens in reality (Appendix B). This will also have an effect on the evaporation, as less water will be available in the catchment.

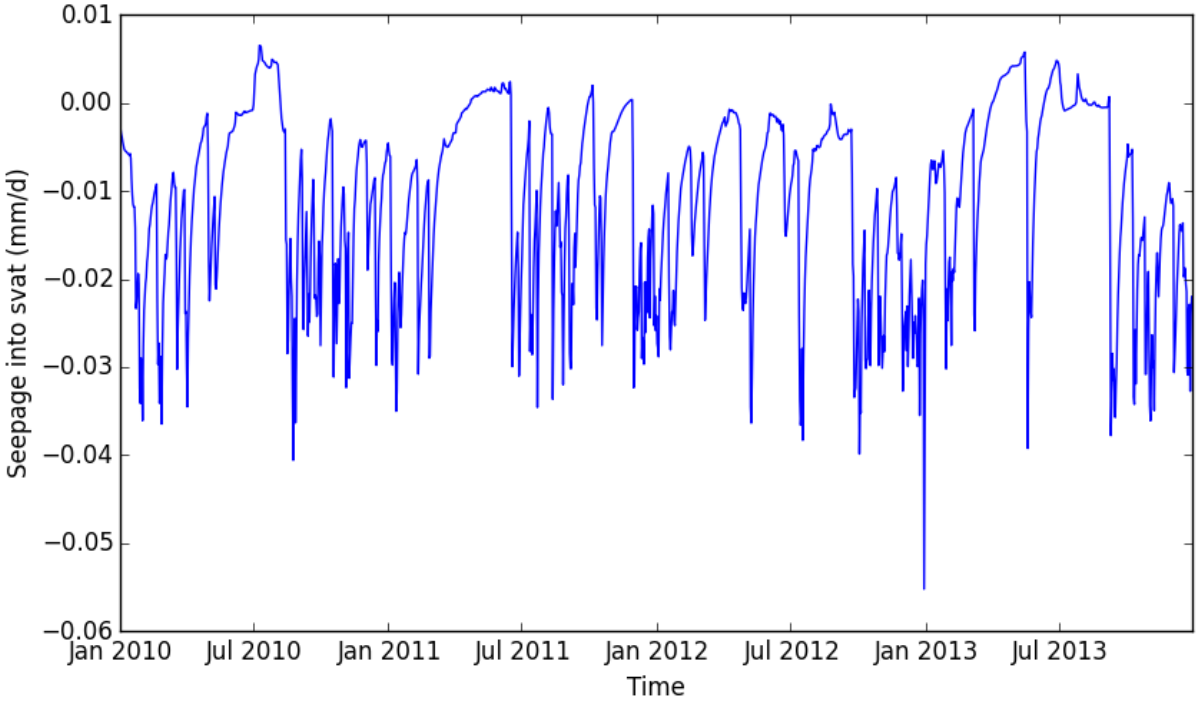

Figure 4-14 Seepage into the SVAT unit of Cabauw. Negative seepage means infiltration into deeper groundwater.

Finally, when comparing the modelled discharge to measurements (Figure 4-15) the performance is mediocre (NS efficiency: -0.979, log-NS efficiency: 0.597). Peaks are modelled too high, around 2 to 3 times higher than the observed peaks. During the summer peaks are not modelled, and the reservoir slowly drains. Some of the differences, mainly the negative discharge peaks in summer, are not modelled correctly due to the net observed discharge being compared to the modelled discharge. The baseflow trend is generally modelled well.

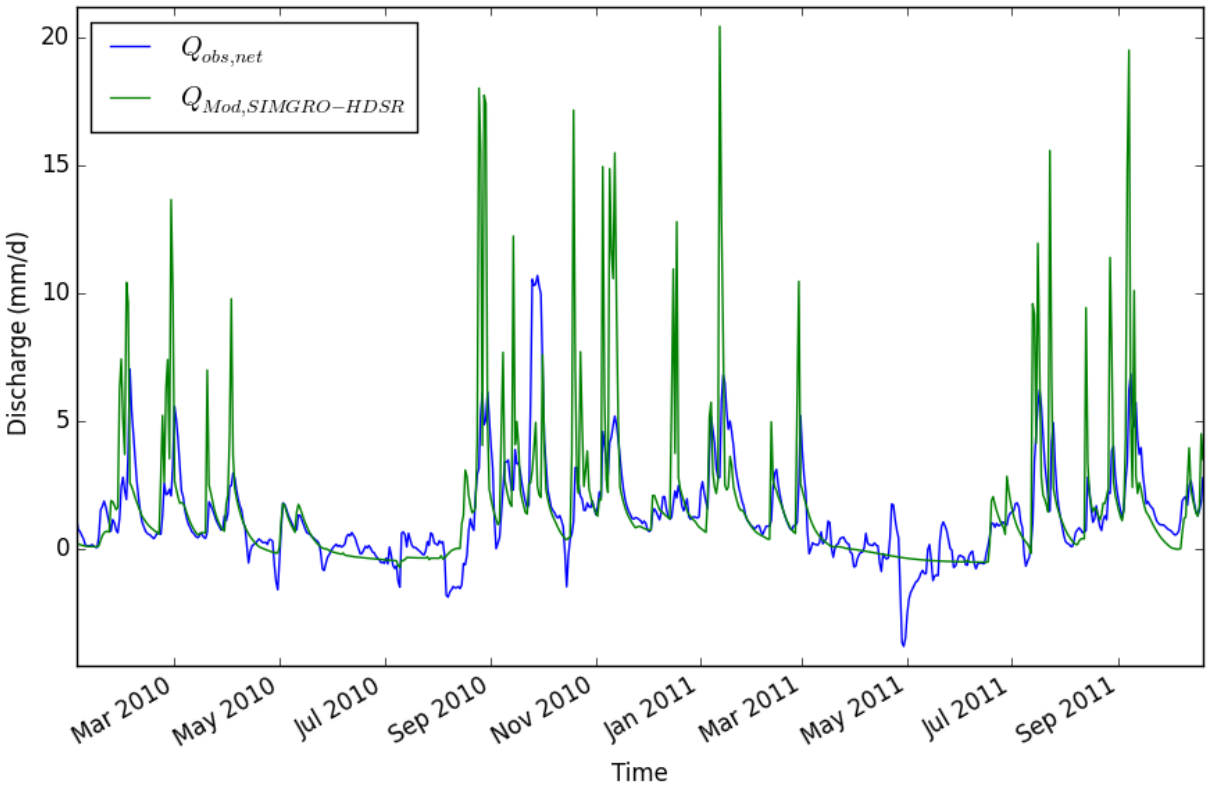

Figure 4-15 SIMGRO-HDSR modelled discharge compared to the observed discharge of the Cabauw polder (2010-2011)

Due to the large differences with reality , and the difficulty of adjusting a model consisting of 300,000 different units, an analysis of imposing actual evaporation has not been done on this model.

4.2.2 SIMGRO-Single Cell

For input data of the single cell model, local precipitation, Makkink evaporation and (eddy covariance) actual evaporation, is used. The studied period is 2007 to 2011, because of the available discharge measurement data. For this reason the eddy covariance actual evaporation data has to be used, as the LSA SAF data is only available from 2011.

When running the one cell model, it seems to have similar problems as the SIMGRO-HDSR model. Water stress occurs quickly during slightly dry periods, which in turn leads to evaporation reduction (Figure 4-16), although it is less severe than with the SIMGRO-HDSR model.

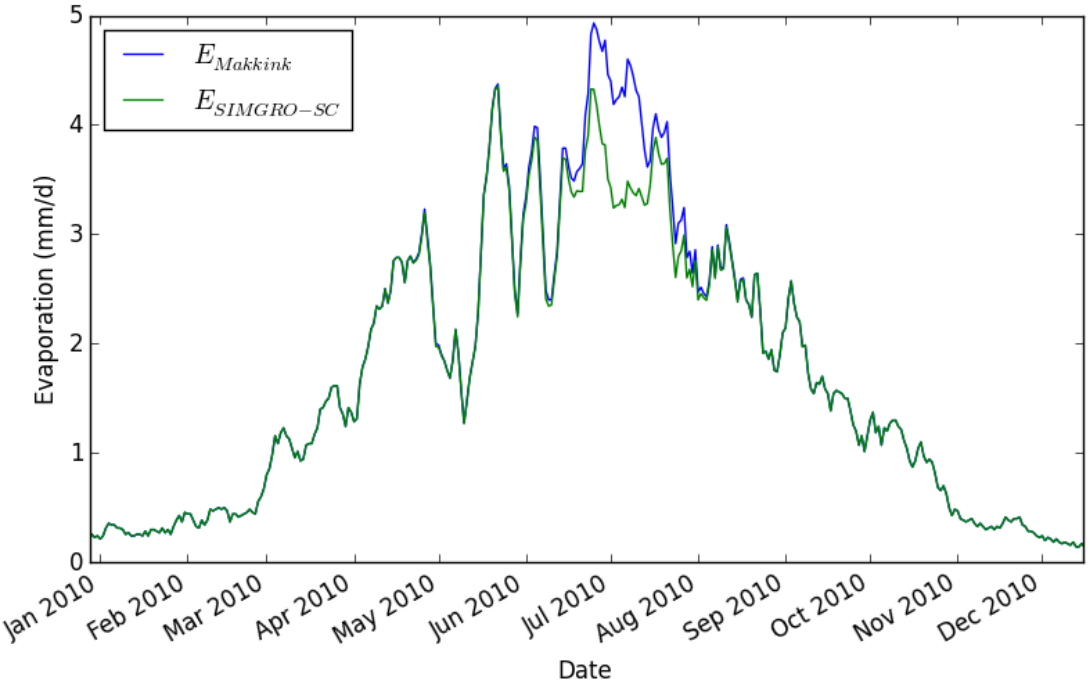

Figure 4-16 Makkink evaporation and SIMGRO-Single Cell calculated actual evaporation, 7 day moving average.

When using the default model structure and parameters for modelling the discharge, the performance is quite poor (Figure 4-17, NS efficiency: 0.480, log-NS efficiency: 0.447). The general trend is modelled, but the intensity of peaks is not accurate. The discharge is also capped at 5 mm/day in the SIMGRO-Single Cell model, due to that being the maximum discharge when the soil is fully saturated. During summers the performance is not optimal due to the modelled discharge being compared to the net discharge, as previously explained.

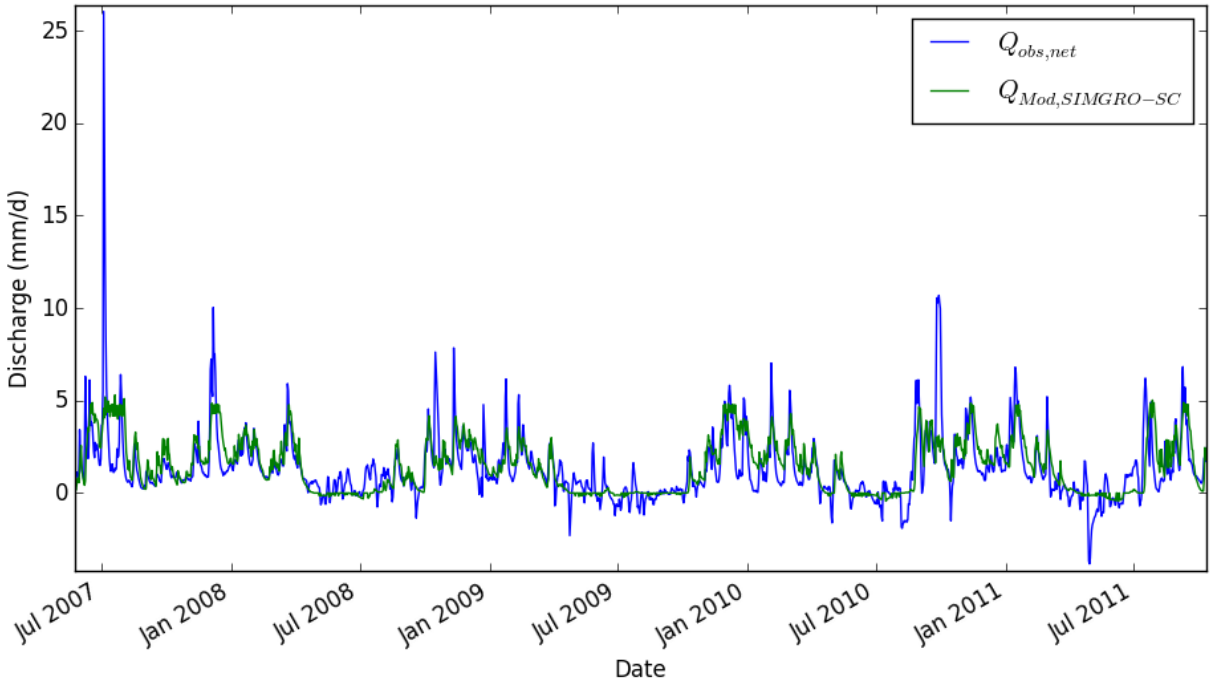

Figure 4-17 Modelled and observed discharge at Cabauw, from 2007 to 2011. NS: 0.480, log-NS: 0.447

To improve the performance of the model, an attempt was made to change and calibrate some of the accessible parameters, namely the drainage parameters (drainage resistance, entry resistance, infiltration resistance, exit resistance) and scaling parameters for the soil moisture and hydraulic conductivity. This was not done at the start, as many of the parameters in SIMGRO are 'physical' parameters which can be observed and measured. Other parameters were based on previous research. The parameters were put in a Monte Carlo simulation, to try to find which ones could improve the model (Figure 4-18).

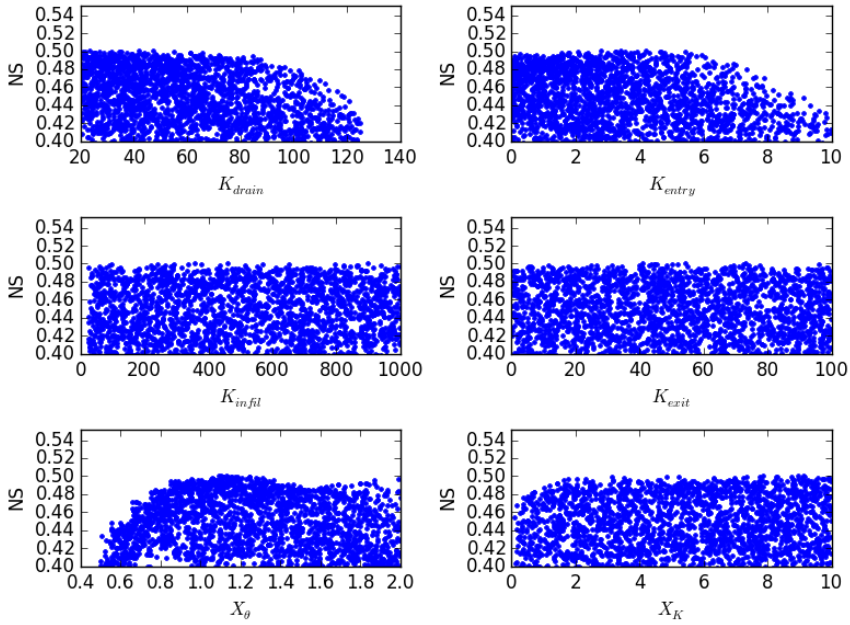

Figure 4-18 Sensitivity plot for the calibration parameters of the SIMGRO-SC model.

The optimal NS-efficiency was only 0.501, barely higher than the non-calibrated model. Calibration did not make much of a difference on the discharge (Figure 4-19).

All parameters had a limited effect on the model. The more important soil parameters were not directly accessible, only through soil types (based on 'BOFEK2012', a soil physical units map (de Vries, 2012)), but even when trying the other soil types, the performance did not significantly improve.

Therefore it seems that it are not the parameters of the model that are the cause of the low performance, but the model structure. In SIMGRO flow through the unsaturated zone uses an implementation of the Richards equation (van Walsum et al., 2010), which assumes a uniform soil. Saturated flow towards drains follows equations based on Darcy's Law, which also assumes a uniform soil. These equations do not take preferential flow paths into account, while this has a large effect on how the unsaturated zone behaves (Beven and Germann, 1982). Flow paths such as animal burrows, soil cracks and gullies have all been observed at Cabauw (Brauer et al., 2014a).

Due to the low performance of the model, and the extreme similarity of the actual and Makkink evaporation at Cabauw, imposing actual evaporation barely makes a difference in the model. However the actual evaporation data does show that the polder does not experience water stress during dry periods, while by default the model does have water stress in dry summers. This is another simple indication that either the model parameterization or structure is wrong.

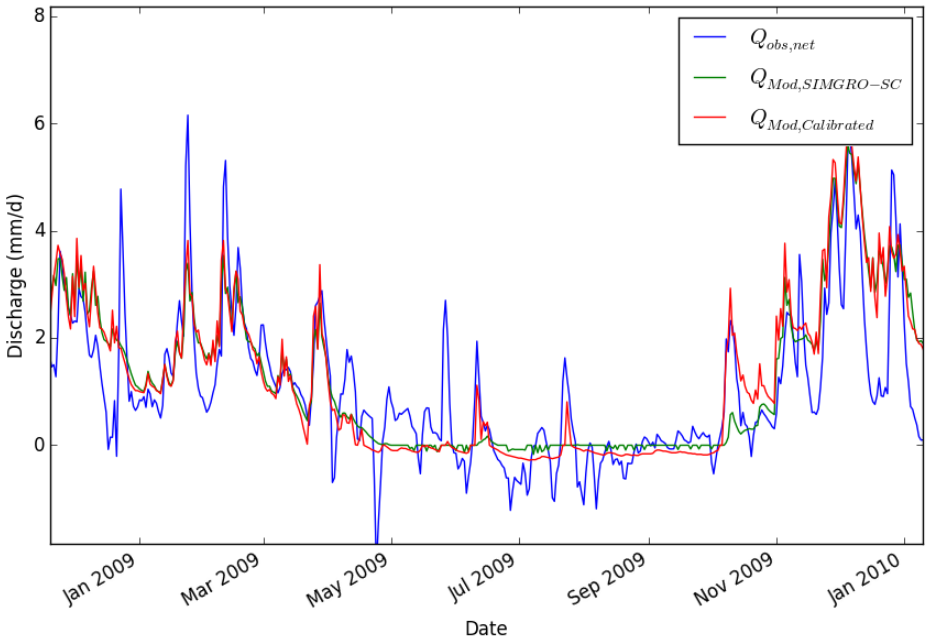

Figure 4-19 Modelled (uncalibrated and calibrated) and observed discharge at Cabauw, during 2009

4.2.3 SIMGRO Summary

When looking at the SIMGRO models, large flaws are uncovered. The models do not represent reality well enough, and show water stress in the Cabauw polder. This is shown when comparing the model calculated actual evaporation to local measurements; the model reduces the evaporation taking place. When looking at the discharge, the performance is also mediocre and does not get the intensity of the peaks correct.

While a calibration of the large HDSR model was not feasible (due to the long runtime), a single cell model was used for a more detailed look at Cabauw. This model performed different than the HDSR model, mainly getting the general trend of the discharge correct, while not getting the peaks and quick regression to the baseflow right. A calibration was attempted, but this did not make much of a change. The main problem with the performance seems to lie in the model structure, namely the assumption of a uniform soil, while not taking preferential flow paths into account.

Due to the low performance of the models, imposing actual evaporation onto the model would not make much of a difference. The limiting factor to the performance of the SIMGRO model seems to be the model structure, and not the quality and accuracy of the input data.

4.3 FLEX

4.3.1 Ubierna river

In the observed discharge of the Ubierna river an error was found, from September to January 2012 the discharge was completely constant and had no peaks at all, while precipitation events did occur. Therefor this part of the data was removed from the dataset, and not be taken into account during the validation period.

When comparing the Makkink reference evaporation at the meteorological station to the LSA SAF actual evaporation of the Ubierna catchment (Figure 4-20), the LSA SAF evaporation shows a lot of moisture stress. Only in the start of summer the evaporation is near the Makkink evaporation. After June/July the soil seems to be dried out, and a low amount of evaporation takes place until

the rains in late autumn provide water again.

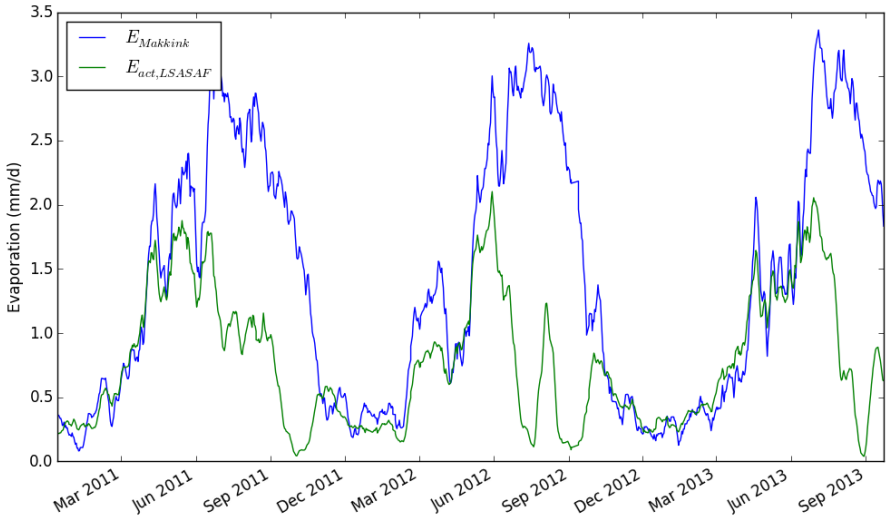

Figure 4-20 Comparison between LSA SAF actual and Makkink reference evaporation the Ubierna catchment

When looking at the water balance for the catchment (Figure 4-21) the water balance does not close. The sum of actual evaporation and discharge is too low compared to the precipitation.

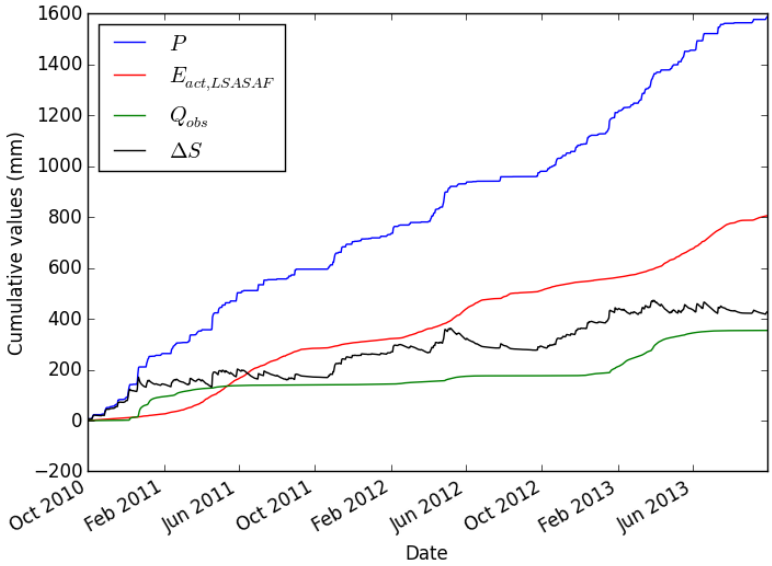

Figure 4-21 Cumulative precipitation ($\mathbf{P}$), actual evaporation ($\mathbf{E}_{act}$), observed discharge ($\mathbf{Q}_{obs}$) and sum of these fluxes (ΔS). Values for the Ubierna river catchment

As the meteorological station is close to the catchment, and the landscape is quite uniform, the precipitation is assumed to be accurate. The discharge is measured in a stream without a fixed structure, and can therefore be very inaccurate. To close the water balance the discharge was multiplied by a factor 2 (Figure 4-22).

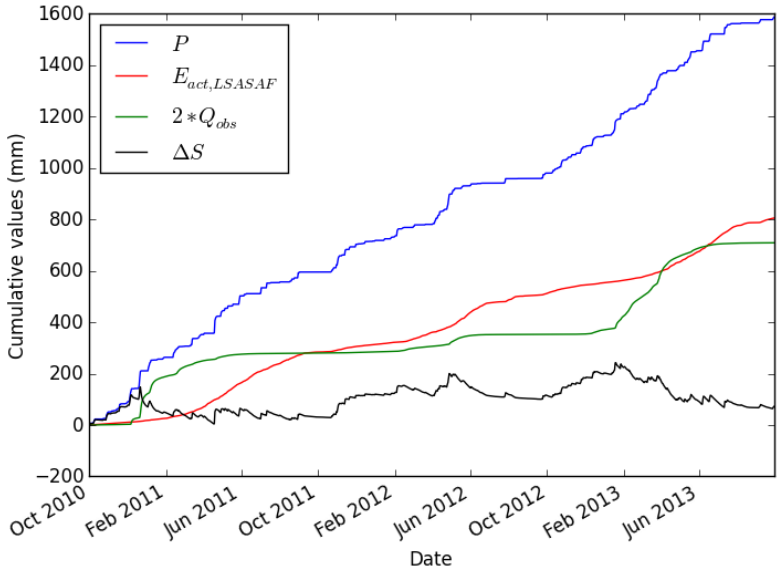

Figure 4-22 Cumulative precipitation ($\mathbf{P}$), actual evaporation ($\mathbf{E}_{act}$), increased observed discharge ($\mathbf{2*Q}_{obs}$) and sum of these fluxes (ΔS). Values for the Ubierna river catchment

The model is then run on the calibration period (October 2010 – October 2011), using both the actual as the Makkink evaporation. The run with the best log-NS efficiency is chosen and then run for the remaining time. The optimal parameters and sensitivity plots are shown in Appendix H.

During the calibration period the LSA SAF actual evaporation seems to do much better according to the log-NS efficiency (Table 4-6), but the difference seems to be more moderate when visually comparing the discharge (Figure 4-23). In the validation period the model using LSA SAF evaporation outperformed the model using Makkink evaporation significantly. Not all peaks that occur in the observed discharge show up in the modelled discharge, and vice versa, but this can be explained by the heterogeneity of the precipitation.

Table 4-6 Calibration and validation parameters for the Ubierna model

	Log-NS Calibration	Log-NS Validation
LSA SAF actual evaporation	0.805	0.787
Makkink evaporation	0.647	0.698

It should be kept in mind however, that the water balance was closed using the LSA SAF actual evaporation data; the data is not completely independent. The addition of a calibration factor for the discharge was attempted (instead of setting it to the previously found factor 2), but this did not improve the performance of the model using Makkink evaporation, of which the log-NS efficiency stayed under 0.700.

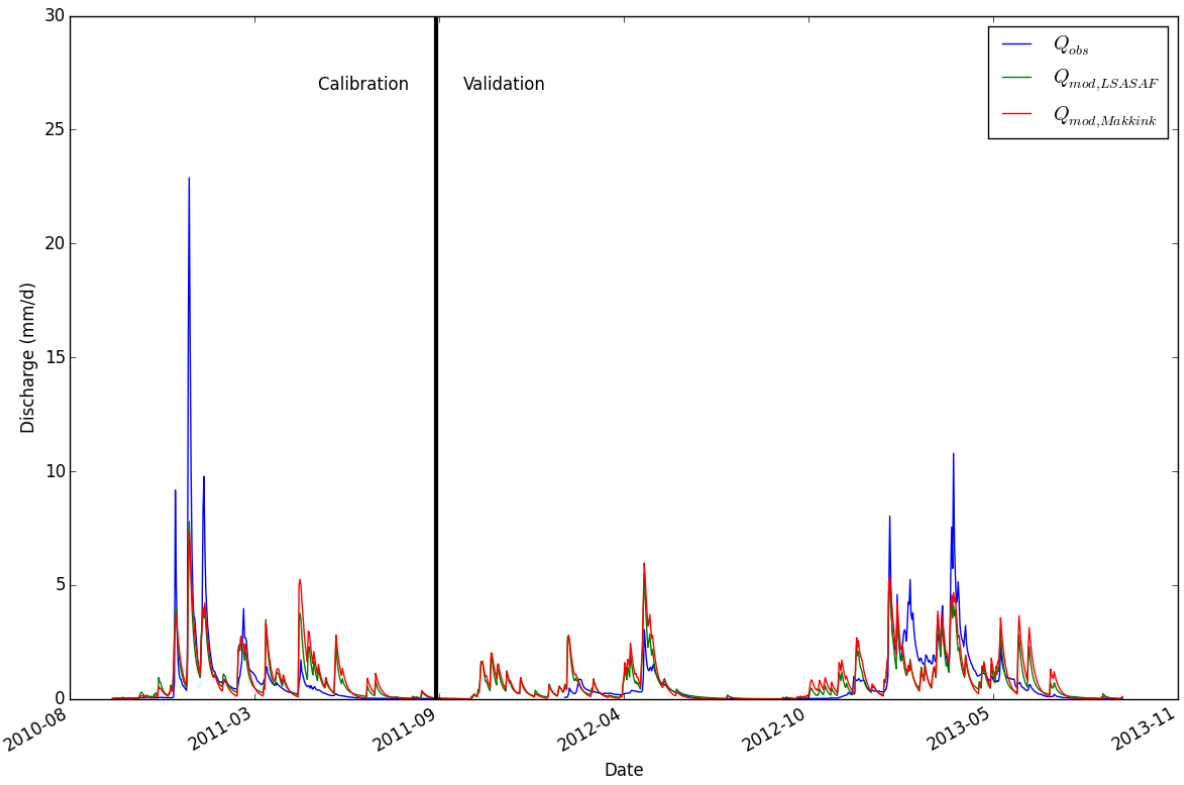

Figure 4-23 Discharge comparison for the Ubierna model. Comparing the observed discharge ($\mathbf{Q}_{obs}$) to the discharge modelled using the LSA SAF evaporation ($\mathbf{Q_{mod,\ LSA\ SAF}}$) and Makkink evaporation ($\mathbf{Q_{mod,\ Makkink}}$)

When comparing the LSA SAF actual evaporation to the FLEX modelled evaporation (Figure 4-24), they seem to be quite similar. The LSA SAF evaporation is generally higher than the modelled evaporation which seems to be reduced due to water stress very early in the summer already.

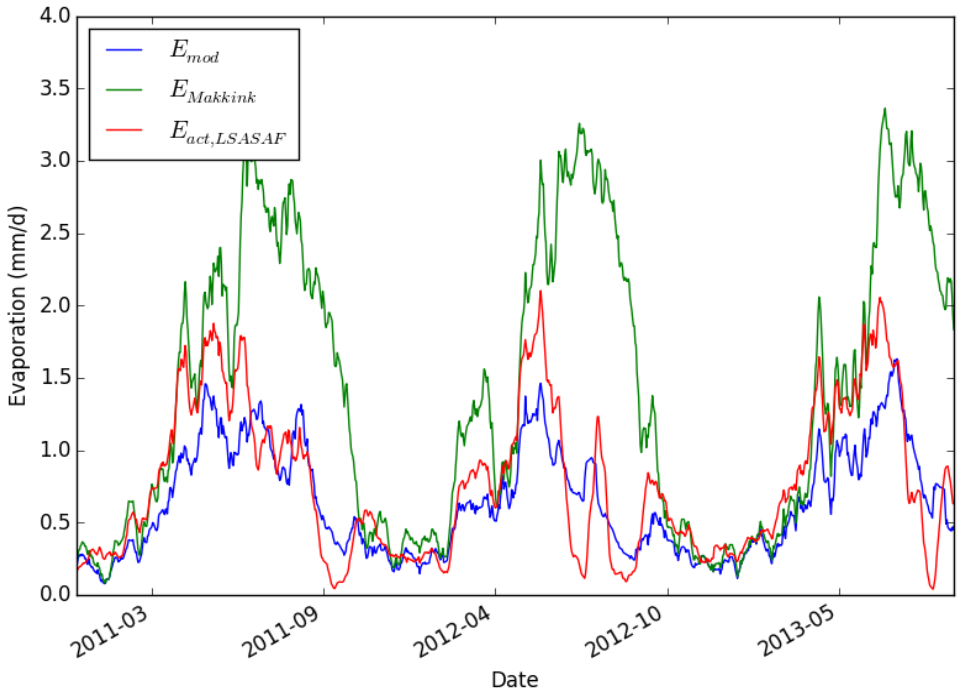

Figure 4-24 Evaporation comparison for the Ubierna model. Comparing the modelled evaporation ($\mathbf{E}_{mod}$) to the Makkink evaporation ($\mathbf{E}_{Makkink}$) and the LSA SAF actual evaporation ($\mathbf{E}_{\mathbf{act,LSA\ SAF}}$).

4.3.2 Ulzama river

When comparing the Makkink reference evaporation at the meteorological station of Pamplona to the LSA SAF actual evaporation of the catchment (Figure 4-25), it seems that the LSA SAF evaporation does not show a large amount of moisture stress.

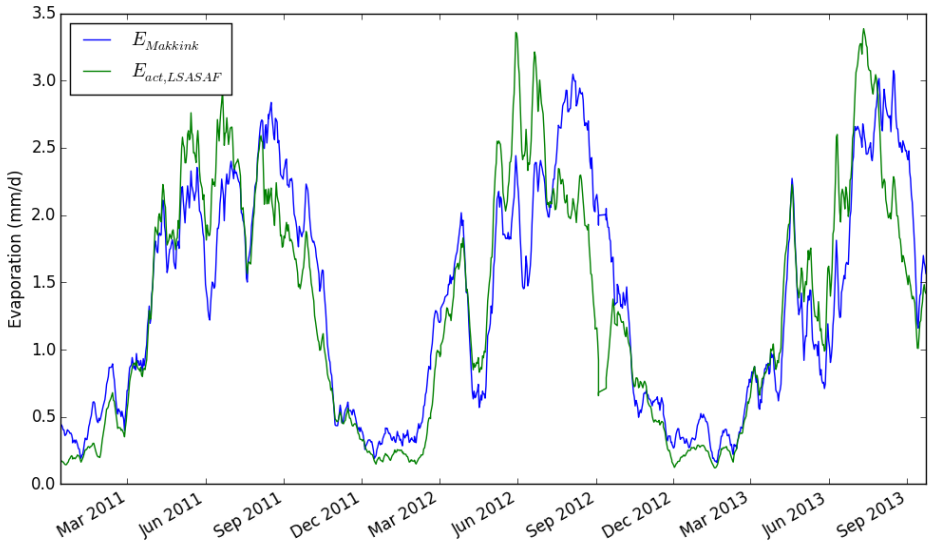

Figure 4-25 Comparison between LSA SAF actual and Makkink reference evaporation the Ulzama catchment

However, when looking at the water balance (Figure 4-26), the values do not add up. The sum of the precipitation, evaporation and discharge leads to a large negative value, meaning that some (or

all) of these values are inaccurate. Of these, the highest uncertainty is probably in the rainfall data; the heterogeneity of rainfall can mean that the actual rainfall in the catchment is much higher, as the meteorological station is located outside of the catchment, in the middle of a valley. As the discharge is measured using a fixed concrete structure, its accuracy will be relatively high.

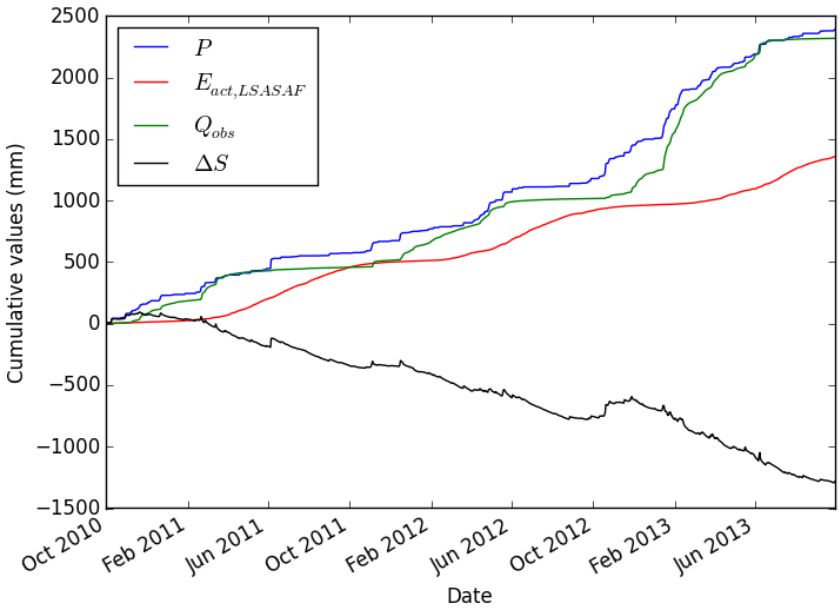

*Figure 4-26 Cumulative precipitation (**P**), actual evaporation ($\mathbf{E}_{act}$), observed discharge ($\mathbf{Q}_{obs}$) and sum of these fluxes (ΔS). Values for the Ulzama river catchment.*

To fix this, the precipitation will be multiplied by a fixed factor, to close the water balance (and assuming that the actual evaporation is correct). The factor used was 1.6, which is in accordance to literature found on correcting precipitation for elevation differences (Panagoulia, 1995). In Figure 4-27 the changed values are shown. The assumption is that generally the same rainfall events happen in the Ulzama catchment as in Pamplona, but with an increased intensity. Calibration of the precipitation factor (for both actual and Makkink evaporation) was attempted, but did not lead to better results than choosing the factor of 1.6 (Appendix H).

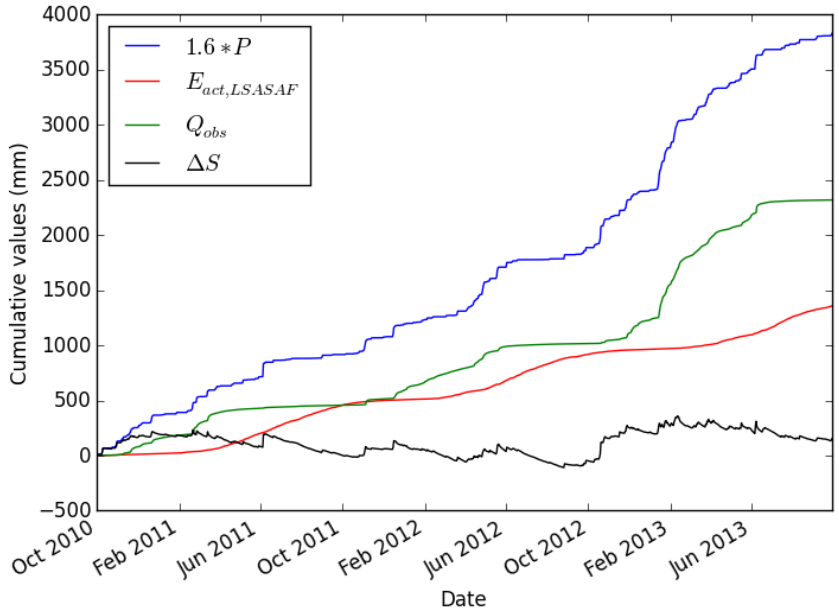

Figure 4-27 Cumulative increased precipitation (1.6$\mathbf{P}$), actual evaporation ($\mathbf{E}_{act}$), observed discharge ($\mathbf{Q}_{obs}$) and sum of these fluxes (ΔS). Values for the Ulzama river catchment.*

The model is then run on the calibration period (October 2010 – October 2011), using both the actual as the Makkink evaporation. The run with the best log-NS efficiency is chosen and then run for the remaining time.

Table 4-7 Calibration and validation parameters for the Ulzama model

	Log-NS Calibration	Log-NS Validation
LSA SAF actual evaporation	0.765	0.769
Makkink evaporation	0.766	0.708

During the calibration period the LSA SAF actual evaporation does not seems to make the model perform better, however performance of the LSA SAF model is better during the validation period (Table 4-7).

The general reaction to precipitation seems to be similar between the models (Figure 4-28), but the difference mainly lies in the first peaks after the dry summer period.

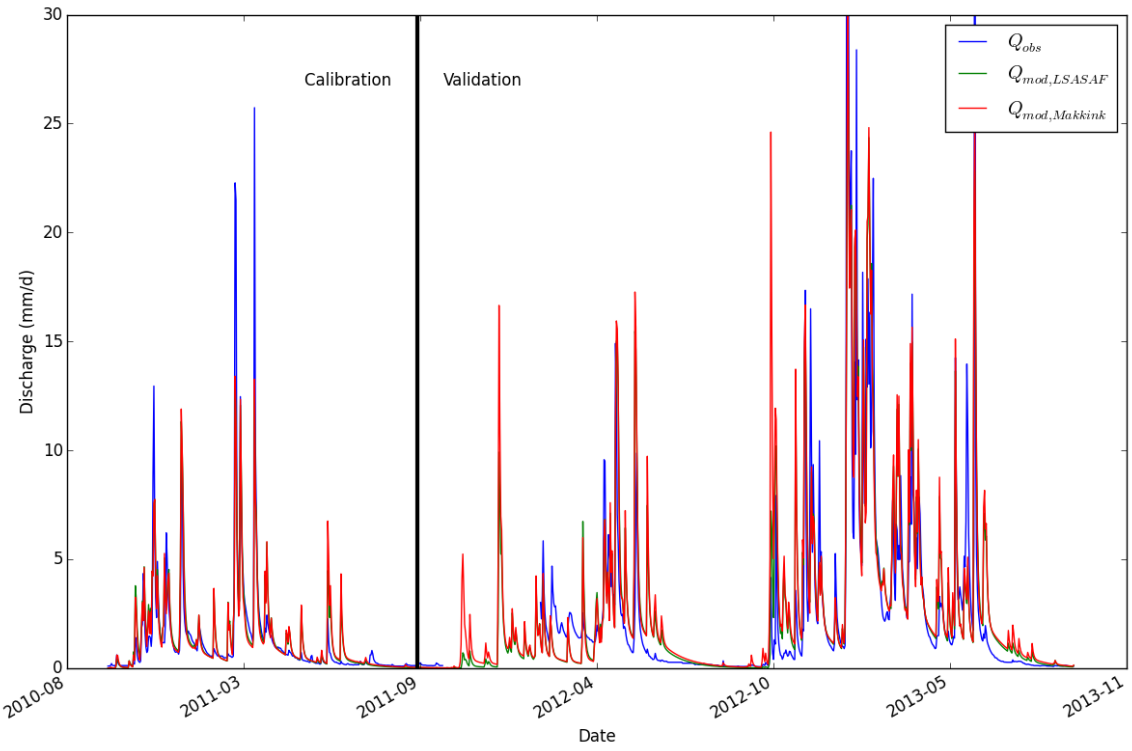

Figure 4-28 Discharge comparison for the Ulzama model. Comparing the observed discharge ($\mathbf{Q}_{obs}$) to the discharge modelled using the LSA SAF evaporation ($\mathbf{Q}_{\mathbf{mod,\ LSA\ SAF}}$) and Makkink evaporation ($\mathbf{Q}_{\mathbf{mod,\ Makkink}}$)

When looking at the evaporation taking place in the models, the model using the Makkink evaporation seems to be experiencing more water stress than the LSA SAF product and is reducing the evaporation more (Figure 42).

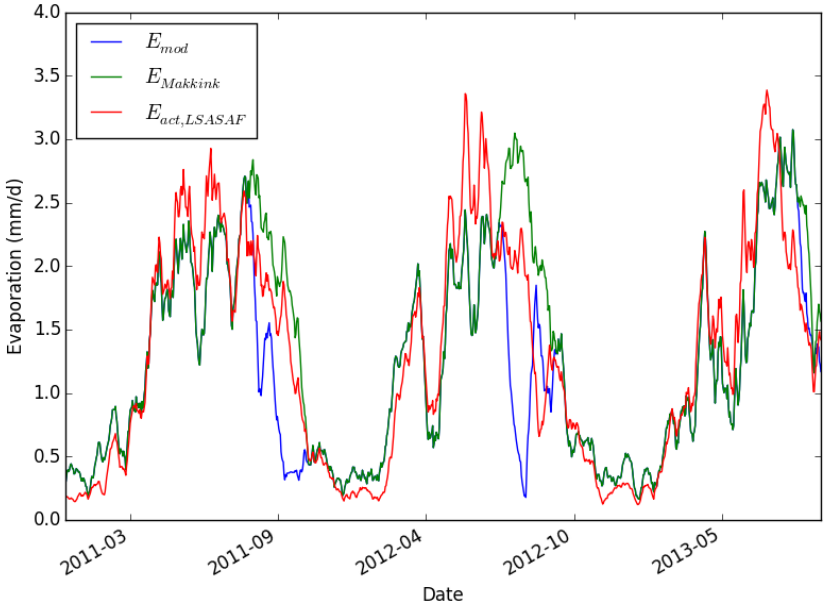

Figure 42: Evaporation comparison for the Ulzama model. Comparing the modelled evaporation ($\mathbf{E}_{\mathrm{mod}}$) to the Makkink evaporation ($\mathbf{E}_{\mathrm{Makkink}}$) and the LSA SAF actual evaporation ($\mathbf{E}_{\mathbf{act,LSA\ SAF}}$).

4.3.3 FLEX Summary

Modelling the Ubierna catchment was successful, although the observed discharge had to be adjusted to make the water balance close. The LSA SAF actual evaporation model seemed to outperform the model using Makkink evaporation significantly. However, the comparison is not without bias, as the correction factor for the discharge was based on the water balance closuring using LSA SAF actual evaporation.

The Ulzama catchment did seem to be modelled well, when looking at the discharges. However it required an adjustment of the precipitation input which could influence the validity of the results. When using the LSA SAF evaporation the model performed well, better than when using the Makkink evaporation.

Both models seemed to perform slightly better when using the LSA SAF actual evaporation. However, to validate this result and ensure this is not due to random chance, local evaporation measurements are needed.

5 Overall Discussion

The first problem of applying actual evaporation lies in determining how accurate the actual evaporation product is. In situ measurements are scarce and the eddy covariance flux measurements that are done are not always accurate enough or openly available (Oak Ridge National Laboratory Distributed Active Archive Center (ORNL DAAC), 2016). Therefore application to a catchment where no in situ actual evaporation measurements have been done will always have a large uncertainty in the accuracy of the remote sensing based actual evaporation. However, the LSA SAF actual evaporation correlated well with the eddy covariance measured actual evaporation at Cabauw (R^2=0.90), and seemed to perform well at the Hupsel Brook and the Spanish catchments.

In previous studies, remote-sensing based evaporation data has mainly been integrated in models, or used as input in simple models. Studies in which the model performance between potential and remote-sensing based actual evaporation has been compared have not been done. It has been shown however, that remote-sensing data could be used to constrain calibration parameters and to reduce equifinality (Silvestro et al., 2015). Besides adding constraints to the calibration, integrating the remote-sensing data into models can lead to a better modelling of river streamflows, and predictions for the future (Parr and Wang, 2015). The possibility of combining remote-sensing based evaporation and soil moisture data to model streamflows in has also been shown (Kunnath-Poovakka et al., 2016).

From this study it seems that the biggest issue with determining if actual evaporation improves models seems to be the need for accuracy of the other components of the model. In the Netherlands (and other areas where water stress is uncommon) the model structure itself needs to be good and realistic enough to see the differences. In more arid areas, the measured discharge and precipitation need to correspond well to the actual discharge and precipitation.

The only catchment for which a good judgement could be made on the added value of the LSA SAF product in hydrological models was the WALRUS model of the Hupsel Brook. Applying the LSA SAF evaporation there did improve the performance when looking at the discharge, but only if the LSA SAF evaporation was corrected to fit the water balance. Once a longer time series of data becomes available, it would become more interesting to look at the Hupsel Brook model again, especially if years with extreme drought occur. That could prove the use of the LSA SAF evaporation if it keeps performing well.

The Cabauw polder, as many areas in the Netherlands was too wet to have any water stress. This is also due to the Water Board wanting to keep the water levels in peat polders high enough to ensure no oxidation of peat takes place, and they actively act to prevent it.

In Spain the uncertainty with the other model inputs (precipitation and discharge) was too high to be able to make a definitive judgement about the performance improvement. Precipitation can be very heterogeneous in intensity, and discharge measurements are too unreliable. Eddy covariance measurements in Spain are also too scarce. However, the models did perform better when using the LSA SAF actual evaporation, and were easy to set up and calibrate. The performance was good, especially considering that no detailed knowledge about the catchments was available.

While the actual evaporation data provided by LSA SAF did show the possibility of improving hydrological models, this improvement is not very useful on its own, as it can only model events in the past, or in real time. The main added value of the actual evaporation data would be to firstly improve the realism of the hydrological model, and to improve the potential evaporation data which is being used. If these things can be done successfully, the predictive qualities of the model under more varying conditions and future scenarios (including climate change) could be improved.

6 Conclusions

The LSA SAF product can give a good representation of actual evaporation, both during clear as well as cloudy conditions, but due to the lack of in situ measurements to compare it to, use of the product can have a large uncertainty, as it does not perform well in every location (LSA SAF, 2011). However, in the studied locations the performance seemed to be sufficient.

In areas in the Netherlands experiencing water stress, using the LSA SAF actual evaporation can give a slight improvement compared to using Makkink evaporation as model input. The Nash-Sutcliffe efficiency of the Hupsel Brook model using LSA SAF actual evaporation was 0.762, compared to 0.733 for the model using Makkink evaporation. Adjusting the actual evaporation to fit the waterbalance was required however. No extremely dry year occurred within the data set, which could have asserted the added value with more certainty.

In areas experiencing no water stress, like the Cabauw polder, the use of actual evaporation is very limited. The equations for potential evaporation are sufficiently accurate that no improvement was found when looking at the catchment discharge if actual evaporation is used. The Nash-Sutcliffe efficiencies for the WALRUS models using actual and Makkink evaporation were 0.693 and 0.673 respectively.

When modelling more arid catchments where there is a lack of detailed knowledge, using the LSA SAF actual evaporation can give a satisfying result. The modelling of the discharges seems to go well, and perform better than when using Makkink evaporation. In the Ubierna catchment the log-Nash-Sutcliffe efficiences were 0.787 for the FLEX model using LSA SAF evaporation, compared to 0.698 for the model using potential evaporation. In the Ulzama catchment the log-Nash-Sutcliffe efficiences were 0.769 for the model using LSA SAF evaporation, compared to 0.708 for the model using Makkink evaporation. Local evaporation measurements could validate these results.

All in all it seems that the LSA SAF evaporation can be applied to hydrological models, with a chance of improvement. The use of remote-sensing based evaporation seems to mainly be in areas experiencing water stress regularly, and in unguaged or badly guaged basins. In those locations applying the LSA SAF evaporation leads to an improvement in model performance.

Appendices

A Determining the land use in the Hupsel Brook

To establish the crop factors which are needed for the Makkink potential evaporation, land use data is needed. To get an accurate estimate the area was inspected using Google Earth. All plots within the catchment were visually inspected, and a classification was chosen (either grass, maize or forest). In Figure A-1 an example is visible.

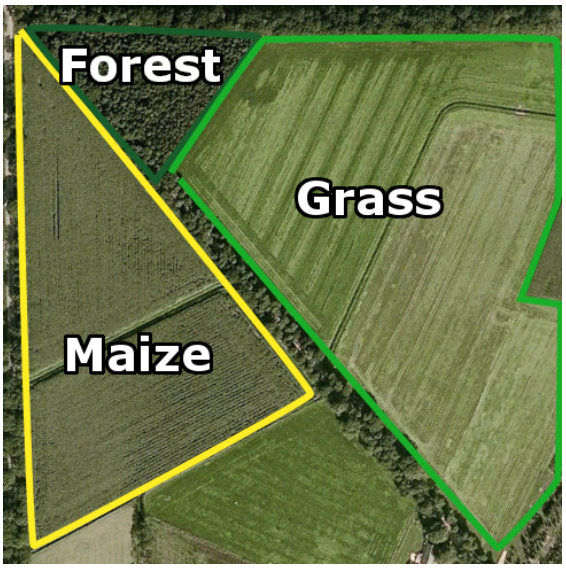

Figure A-1 Land use selection example

These plots were then completely filled in a single colour, each colour corresponding to a land use type. This resulted in Figure A-2. Some gaps exist because of other land use (buildings, industry) but these were deemed small enough to not matter on the catchment scale.

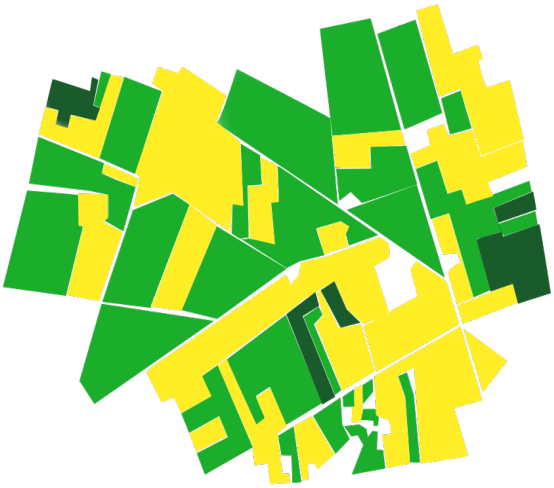

Figure A-2 Land use within the catchment. Colours are the same as in Figure A-1

By digitally analysing the image (using python), and comparing the area of each colour to the total coloured in area, the land use distribution was found. This was 50% grass, 45% maize and 5%

forest.

B Seepage in the Cabauw polder

To get an estimate of the seepage, a time series of groundwater heads is available, based on observations using an observation well from multiple years. This measurement does have a high grade of inaccuracy, and the resistance between the top aquifer and the measured depth is also not accurately known.

Because of the inaccuracy of the seepage, a water balance can be used to determine the yearly seepage, as actual evaporation is determined accurately, and the local rainfall and discharge are both measured at Cabauw. To calculate the seepage the following equation is used:

$$\frac{\Delta S}{\Delta t} = P - E - Q + R \tag{B-1}$$

Where ΔS is the change in storage in the catchment (mm/d), P is the precipitation (mm/d), E is the (actual) evaporation (mm/d), Q is the discharge (mm/d), and R is the seepage (mm/d). Between winters, the storage change can be neglected, as the soil will be completely saturated, and the catchment discharges most of the excess precipitation quickly. This means that on a yearly scale:

$$R = E + Q - P \tag{B-2}$$

In Figure B-1 the remaining term of the water balance is shown. The yearly seepage can be determined by looking the differences from winter to winter, and is equal to 200 to 300 mm per year. This is probably also related to the water levels in the Lek river. When looking at only the winter period, where ΔS is small (on a multiple week timescale) due to the frequent precipitation and low evaporation, the seepage during winter can be found, and is equal to around 0.25mm/day. To make an estimation of the seepage during the year, a sinusoidal shape is assumed, with a seepage of 0.25mm/day during winter, and a total of 250mm/year. This leads to the seepage equation:

$$R(t) = 0.65 \sin\left(\frac{t-45}{365} 2\pi\right) + 0.85 \tag{B-3}$$

Where $R(t)$ is the seepage as a function of t, the day of the year. There is a shift of 45 days to match up the seepage with the water balance.

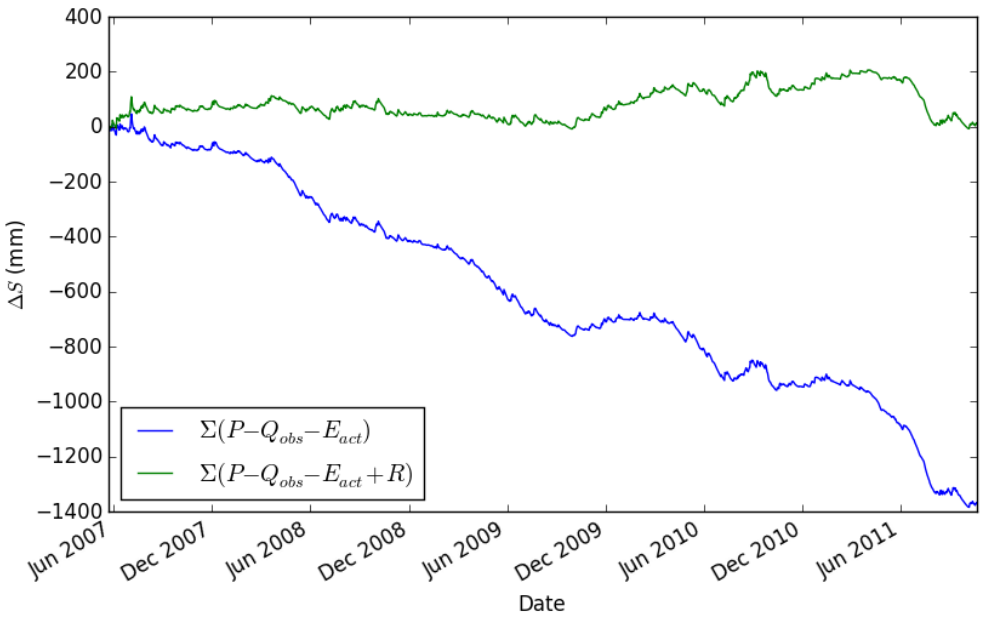

Figure B-1 Water balance closure. Without the derived seepage term (blue) and including the derived seepage term (green)

C Imposing actual evaporation on WALRUS

Due to the open structure of WALRUS in the R programming language, changes can be easily made. In the model code a function is available to redefine the evaporation reduction function. Disabling the reduction is as simple as setting the reduction function to always return *1* (Figure C-1).

```
21  func_beta_dv_normal = cmpfun(function (x)
22  {
23    (1)
24  })
25
26  set_func_beta_dv(func_beta_dv_normal)
```

Figure C-1 Imposing actual evaporation on WALRUS

This will eliminate all evaporation reduction, and make the potential evaporation always be equal to the actual evaporation.

D Imposing actual evaporation on SIMGRO

Imposing actual evaporation in SIMGRO is not directly possible, due to the evaporation reduction function being built into the compiled model code. The only way to remove the evaporation reduction is to adjust the related parameters until it does not take place anymore.

By both increasing the root depth (in the *area_svat.inp* file) and adjusting the Feddes function parameters (in the *luse_svat.inp* file) the evaporation reduction is effectively disabled when looking at Cabauw. This will not work in all cases, especially when looking more arid areas.

In *luse_svat.inp* the parameters which have to be changed are shown in Figure D-1. These are the parameters h_4, h_{3L} and h_{3H} of the Feddes function.

```
1 gras                  1    1    0.00    0.00   -2.00   -8.00  -80.00    5.0    0.1   -3.20
1 gras                  1    1    0.00    0.00 -999.00 -999.00 -999.00    5.0    0.1   -3.20
```

Figure D-1 Change in the luse_svat.inp file to allow imposing actual evaporation

E Influence of soil moisture on errors in LSA SAF

During the comparison of evaporation of the Hoogheemraadschap Stichtse Rijnlanden model with the LSA SAF product, a very low evaporation rate was observed around the Heuvelrug in Utrecht. In a HKV memo this was assumed to be because of a very low LAI (around 2.0), which did differ extremely from other LAI estimations and reasonability, as it is a forested area.To make sure that the leaf area index is the main cause, and not low soil moisture, the data source was investigated to rule it out as cause of the error.

E.1 Soil moisture in the LSA SAF actual evaporation algorithm

In the actual evaporation calculation, the canopy resistance is used. This canopy resistance is related to the linearly related to the soil moisture Jarvis function; $f_2\left(\theta\right) = \frac{\theta - \theta_{\mathrm{pwp}}}{\theta_{\mathrm{cap}} - \theta_{\mathrm{pwp}}}$ (LSA SAF, 2010). θ is the average unfrozen soil water content and is derived from the four-layered ERA-Interim soil moisture data.

E.2 Source of soil moisture data

The soil moisture data comes from the ERA-Interim climate reanalysis (ECMWF, 2016). Data is available between 1979 and 2015, on a daily basis. The spatial resolution is 0.125 degrees (around 14km above the Netherlands). Soil moisture data is modelled for 4 soil layers.

E.3 Comparison of soil moisture between Cabauw and Heuvelrug

Data for the years 2008-2011 was retrieved and the data points for Cabauw and the Heuvelrug extracted. In Figure E-1 the soil moisture in the top layer for all 4 layers, of both locations is shown.

The data shows that in the ERA-Interim model, which is the data source of LSA SAF, there barely is a difference between Cabauw and the Heuvelrug. As such soil moisture can be ruled out as the cause of the low evaporation.

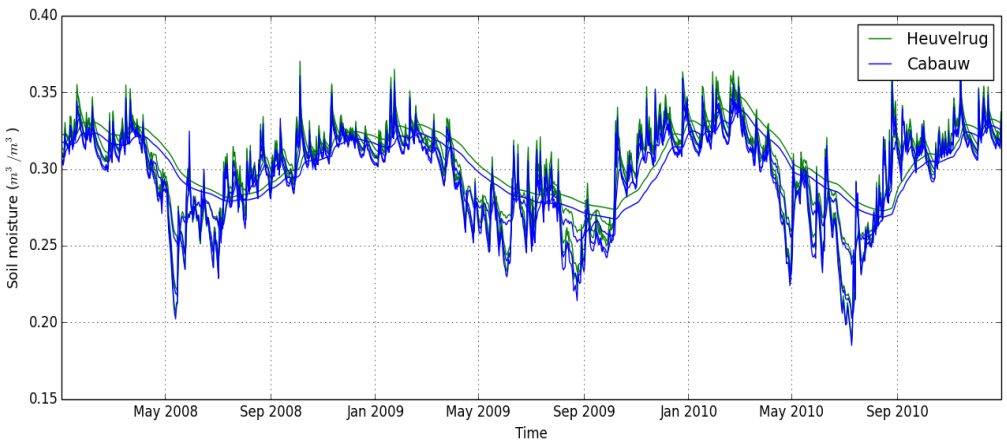

Figure E-1 Soil moisture comparison between Cabauw and the Heuvelrug

F Sensitivity plots WALRUS

The sensitivity plot for the calibration of the Hupsel Brook (with E_{factor}) is shown in Figure F-1. Both the potential and actual evaporation lead to very similar plots, although the main difference is found in the C_W.

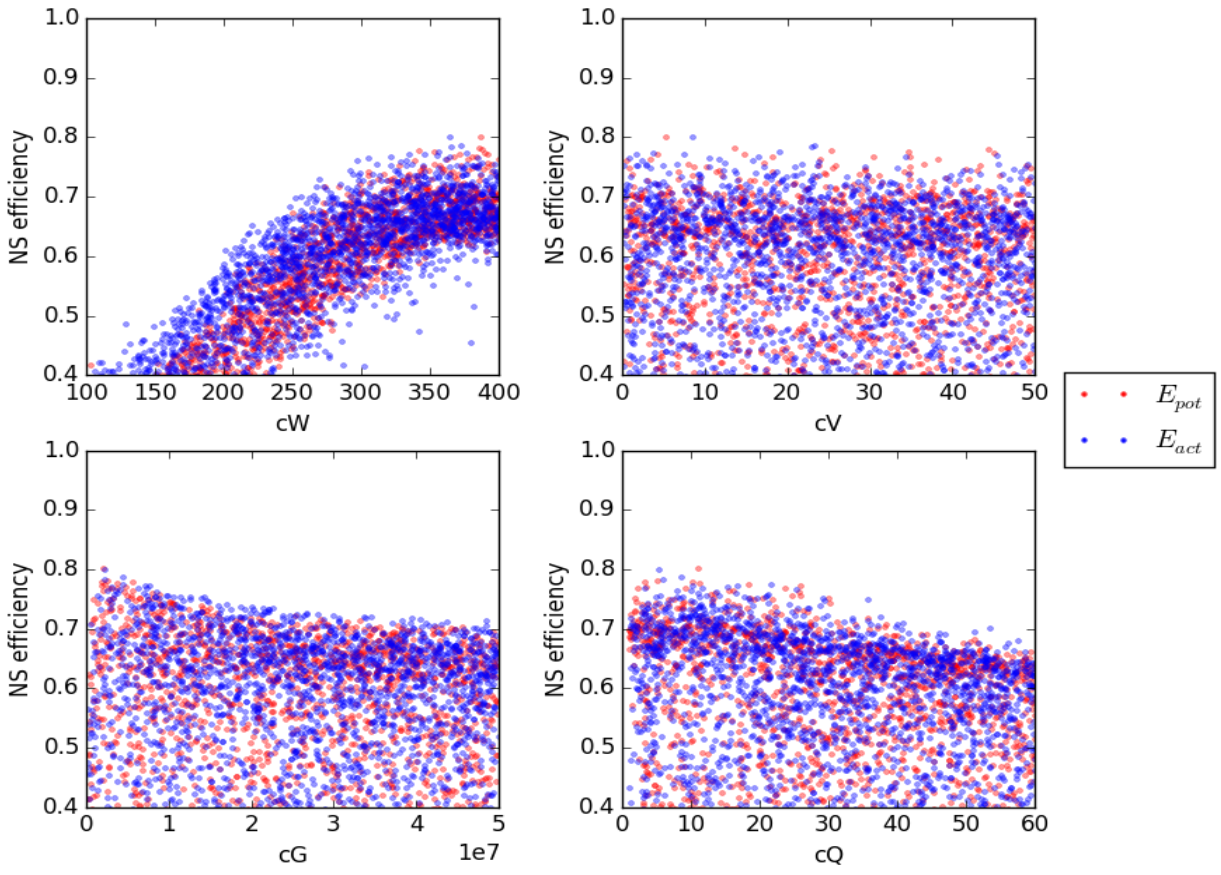

Figure F-1 Sensitivity plots of the Hupsel Brook calibration, with $\mathbf{E}_{factor}$

F.1 Cabauw:

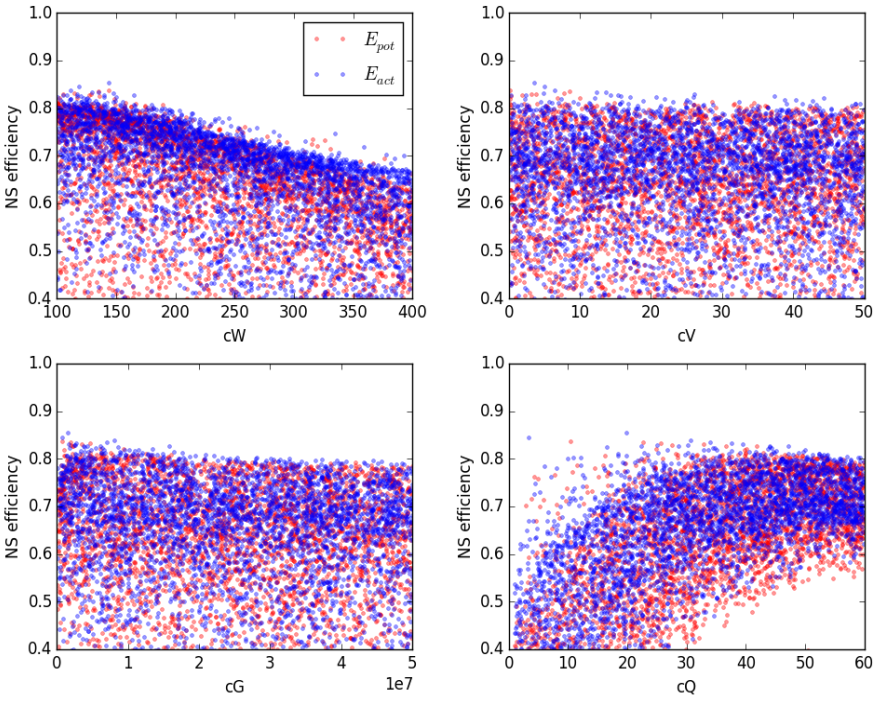

Figure F-2 Sensitivity plots Cabauw calibration. With $\mathbf{E}_{factor}$

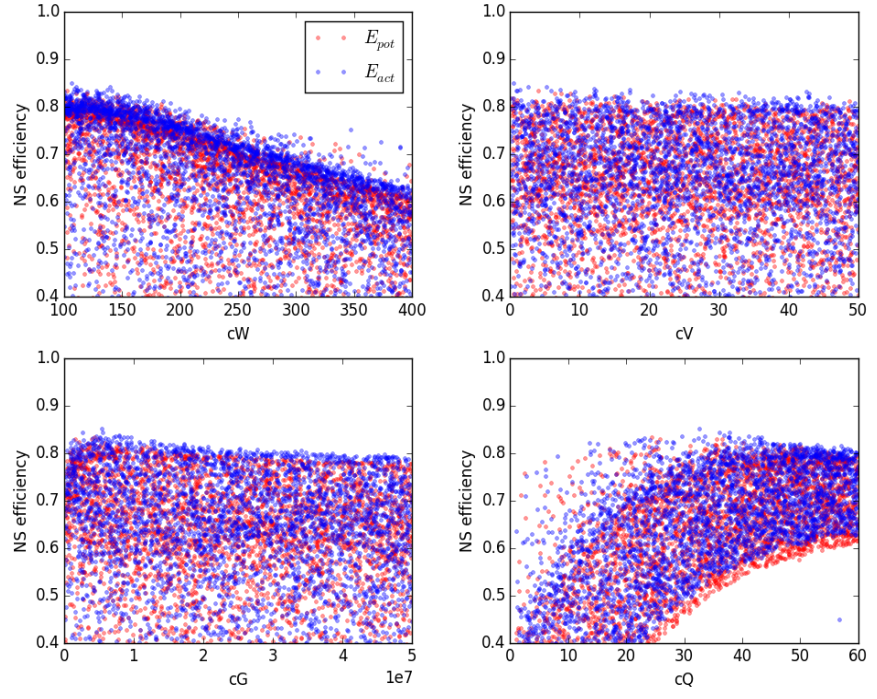

Figure F-3 Sensitivity plots Cabauw calibration. No $\mathbf{E}_{factor}$

G Full page discharge plots

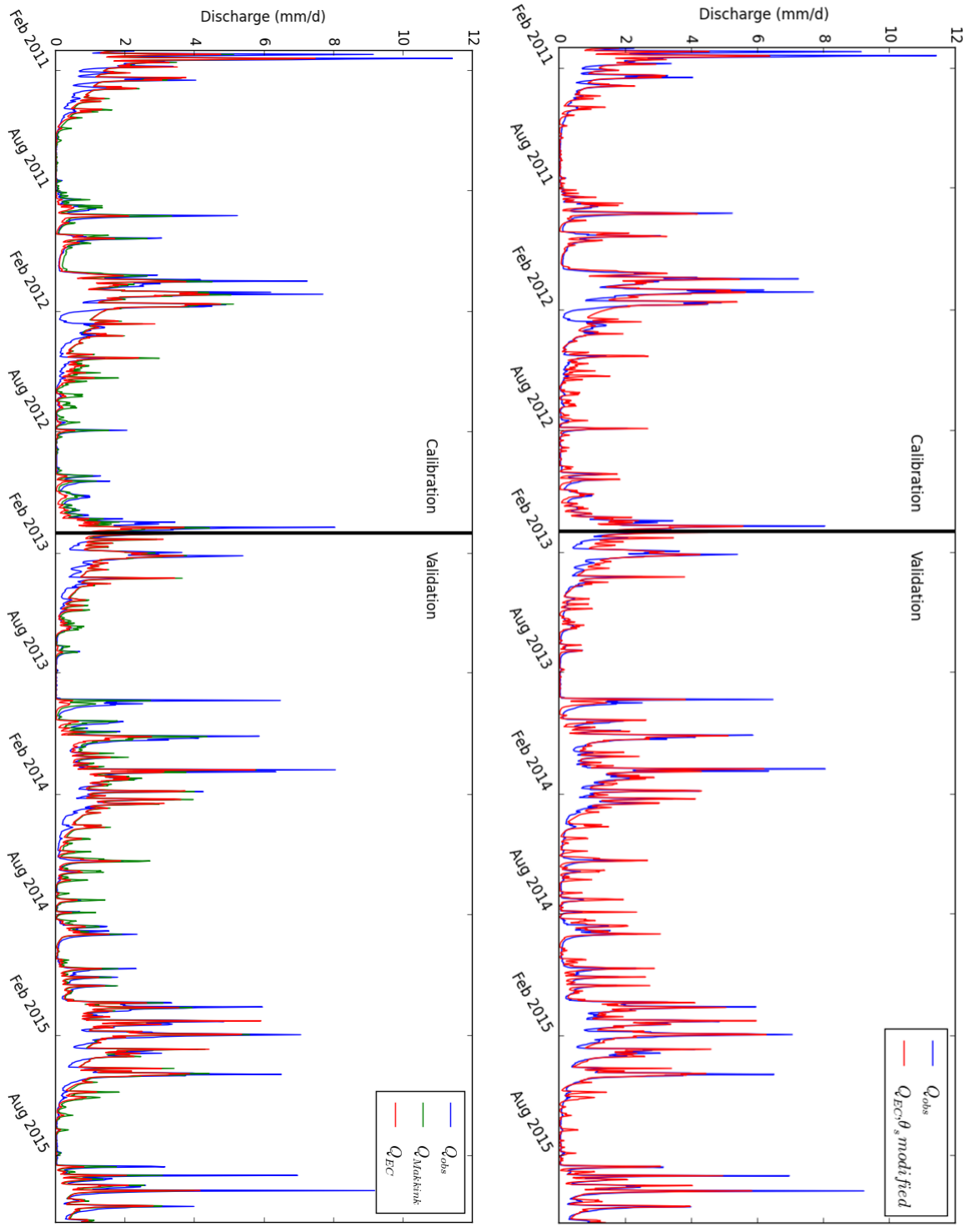

Figure G-1 Left: normal calibration. Right: modified θ_S calibration.

H FLEX calibration

H.1 Ubierna model

The following figures are the sensitivity plots for the calibration using the LSA SAF actual evaporation (Figure H-1) and the Makkink evaporation (Figure H-2).

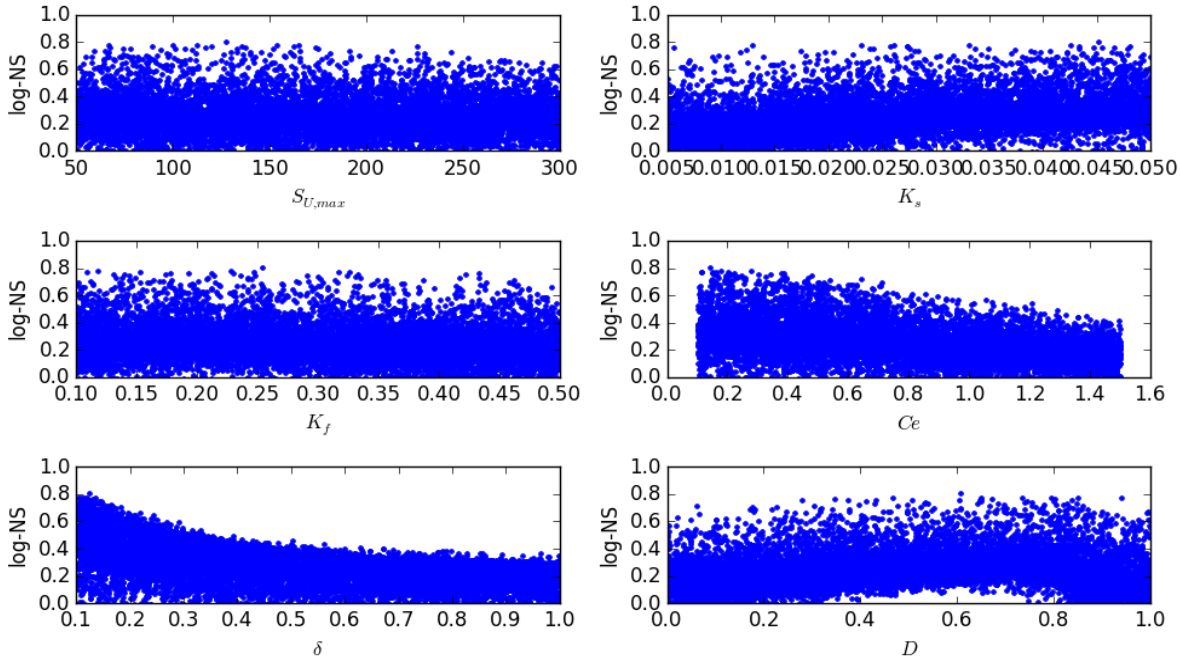

Figure H-1 Sensitivity plot for the Ubierna model. Using the LSA SAF actual evaporation

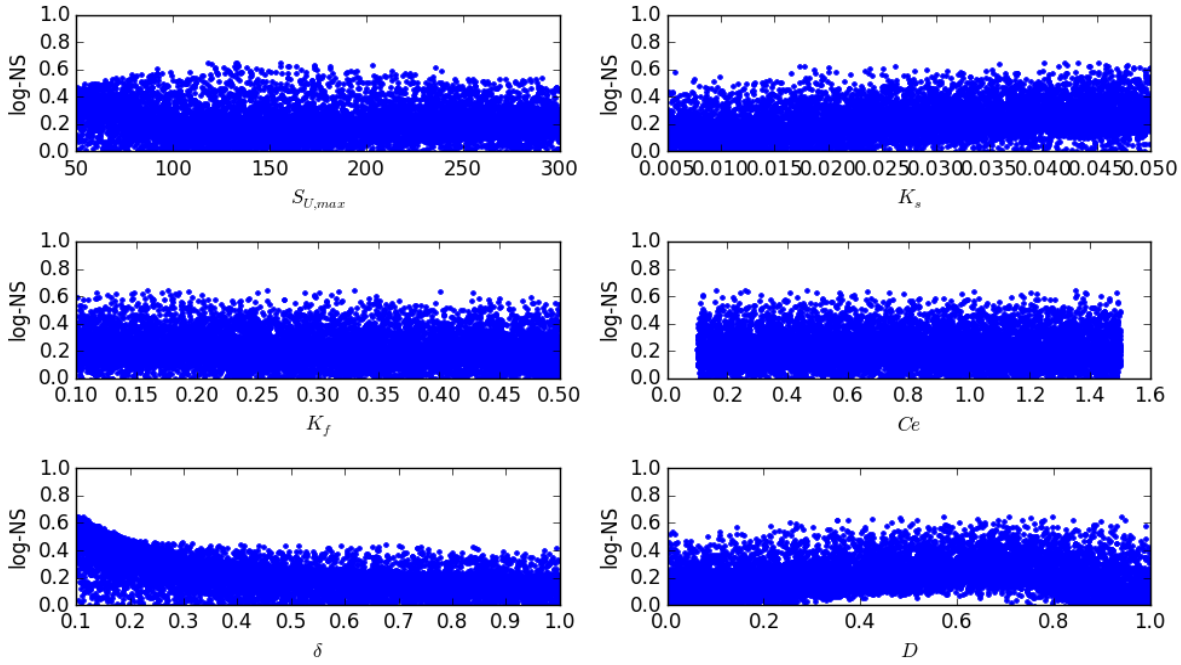

Figure H-2 Sensitivity plot for the Ubierna model. Using Makkink evaporation

The optimal parameter sets of the calibration are shown in Table H-1.

Table H-1 Optimal parameters of the Ubierna calibration

	LSA SAF calibration	Makkink calibration
$S_{U,max}$	127.3	132.5
K_s	0.045	0.045
K_f	0.254	0.159
Ce	0.140	1.350
δ	0.124	0.102
D	0.608	0.940

H.2 Ulzama model

The following figures are the sensitivity plots for the calibration using the LSA SAF actual evaporation (Figure H-3) and the Makkink evaporation (Figure H-4).

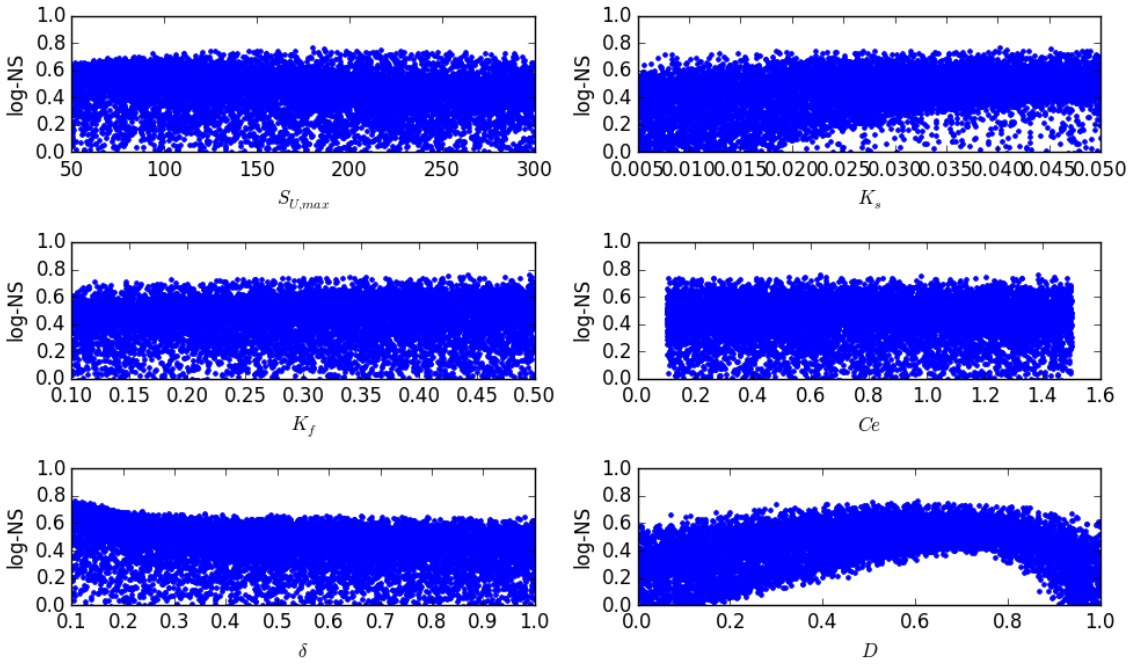

Figure H-3 Sensitivity plot for the Ulzama model. Using the LSA SAF actual evaporation

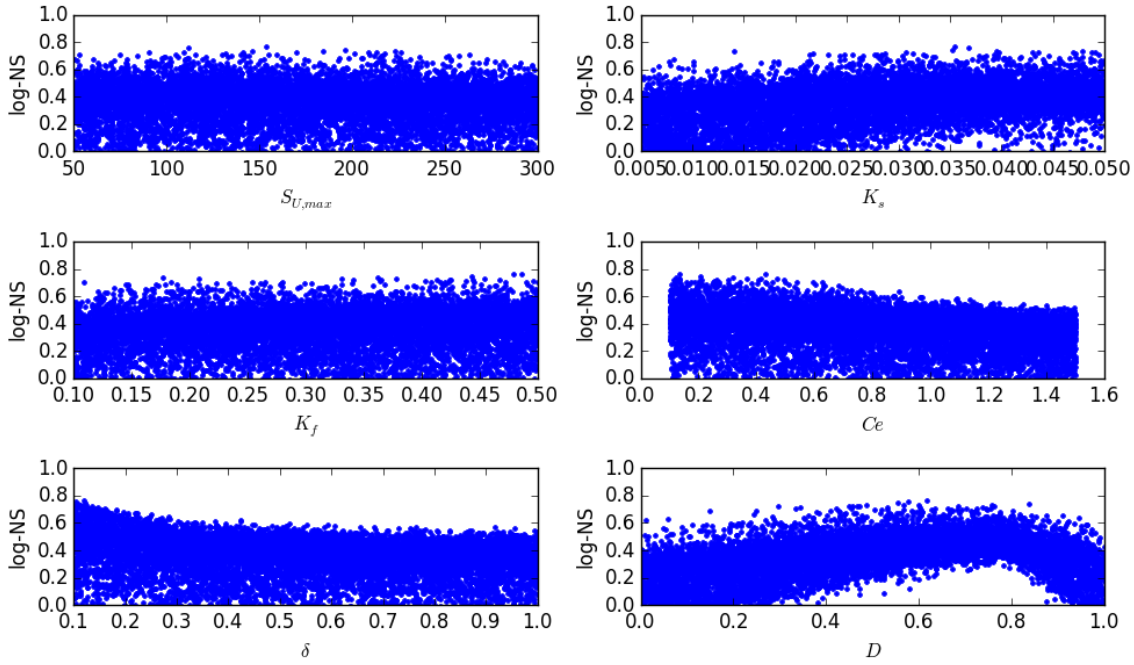

Figure H-4 Sensitivity plot for the Ulzama model. Using Makkink evaporation

The optimal parameter sets of the calibration are shown in Table H-2.

Table H-2 Optimal parameters of the Ulzama calibration

	LSA SAF calibration	Makkink calibration
$S_{U,max}$	179.8	153.9
K_s	0.040	0.035
K_f	0.442	0.486
Ce	1.381	0.134
δ	0.106	0.119
D	0.604	0.616

H.3 Precipitation factor Ulzama

To remove the bias from the comparison in Ulzama (due to the fixed precipitation increase), a sensitivity analysis was done using the potential evaporation and the precipitation factor.

The precipitation factor was added as a calibration parameter, and the model was calibrated (Figure H-5). The maximum calibration log-NS efficiency was 0.835, higher than without the calibrated precipitation factor. However, the validation performance did not improve, and the log-NS-efficiency stayed the same (0.708).

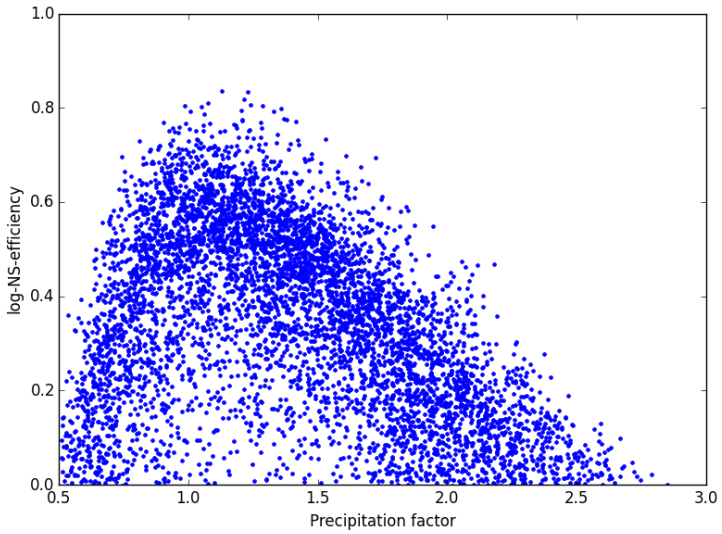

Figure H-5 Sensitivity plot for the precipitation factor calibration using Makkink evaporation

When applying the precipitation factor to the calibration of the model using LSA SAF actual evaporation, the log-NS-efficiency of the calibration was 0.831, with the optimum about a precipitation factor of 1.05. However, the performance of the model during the validation period was very bad, with a log-NS-efficiency of -0.12.

Literature

R. G. Allen, L. S. Pereira, D. Raes, and M. Smith. FAO Irrigation and Drainage Paper No. 56. Technical report, FAO, Rome, 1998. URL http://www.fao.org/docrep/x0490e/x0490e0b.htm.

R. P. Bartholomeus and J. Witte. Gewasfactoren en potentiële verdamping: geen robuuste combinatie. Het gebruik van gewasfactoren in klimaatprojecties. Technical report, KWR, 2013.

W. Bastiaanssen, H. Pelgrum, J. Wang, Y. Ma, J. Moreno, G. Roerink, and T. van der Wal. A remote sensing surface energy balance algorithm for land (SEBAL): 2. Validation. *Journal of Hydrology*, 212-213:213–229, 1998. ISSN 00221694. doi: 10.1016/S0022-1694(98)00254-6. URL http://www.sciencedirect.com/science/article/pii/S0022169498002546.

K. Beven and P. F. Germann. Macropores and water flows in soils. *Wat. Resour. Res.*, 18(5):1311–1325, 1982. ISSN 00431397. doi: 10.1029/WR018i005p01311.

F. C. Bosveld. A quality controled and gap-filled data set for Cabauw for the period 2001 - today, 2014. URL http://www.cesar-database.nl/ShowSystemDescription.do?datasetID=1159.

I. S. Bowen. The ratio of heat losses by conduction and by evaporation from any water surface. *Physical Review*, 27(6):779–787, 1926. ISSN 0031899X. doi: 10.1103/PhysRev.27.779.

C. C. Brauer, A. J. Teuling, P. J. J. F. Torfs, and R. Uijlenhoet. The Wageningen Lowland Runoff Simulator (WALRUS): A lumped rainfall-runoff model for catchments with shallow groundwater. *Geoscientific Model Development*, 7(5):2313–2332, 2014a. ISSN 19919603. doi: 10.5194/gmd-7-2313-2014.

C. C. Brauer, P. J. J. F. Torfs, A. J. Teuling, and R. Uijlenhoet. The Wageningen Lowland Runoff Simulator (WALRUS): Application to the Hupsel Brook catchment and the Cabauw polder. *Hydrology and Earth System Sciences*, 18(10):4007–4028, 2014b. ISSN 16077938. doi: 10.5194/hess-18-4007-2014.

G. Burba. Representation of eddies passing a measurement tower, 2008. URL https://commons.wikimedia.org/wiki/File:Py{%}C3{%}B6rrekovarianssi-tekniikan{_}kaaviokuva.jpg.

G. Burba. *Eddy Covariance Method for Scientific, Industrial, Agricultural, and Regulatory Applications*. LI-COR Biosciences, Lincoln, USA, 2013.

Cesar Consortium. Cesar Database, 2016. URL http://www.cesar-database.nl/.

H. A. R. De Bruin and W. N. Lablans. Reference crop evapotranspiration determined with a modified Makkink equation. *Hydrological Processes*, 12(7):1053–1062, 1998. ISSN 08856087. doi: 10.1002/(SICI)1099-1085(19980615)12:7<1053::AID-HYP639>3.0.CO;2-E.

Q. de Jong van Lier, J. C. van Dam, K. Metselaar, R. de Jong, and W. H. M. Duijnisveld. Macroscopic Root Water Uptake Distribution Using a Matric Flux Potential Approach. *Vadose Zone Journal*, 7(3):1065, 2008. ISSN 1539-1663. doi: 10.2136/vzj2007.0083. URL http://www.scopus.com/inward/record.url?eid=2-s2.0-44949169662{&}partnerID=tZOtx3y1.

F. de Vries. Bodemfysische Eenhedenkaart (BOFEK2012), 2012. URL http://www.wageningenur.nl/nl/show/Bodemfysische-Eenhedenkaart-BOFEK2012.htm.

P. Droogers. Verbetering bepaling actuele verdamping voor het strategisch waterbeheer. Technical report, STOWA, Utrecht, 2009. URL http://www.stowa.nl/Upload/publicaties/Rapport2009-11{_}LR.pdf.

ECMWF. ERA Interim, Daily data, 2016. URL http://apps.ecmwf.int/datasets/data/interim-full-daily/.

R. Feddes, P. Kowalik, and H. Zaradny. *Simulation of field water use and crop yield*. PUDOC / Centre for Agriculture Publishing and Documentation, Wageningen, 1978. ISBN 902200676X, 0470264632.

T. Foken. The energy balance closure problem: an overview. *Ecological Applications*, 18(6):1351–1367, sep 2008. ISSN 1051-0761. doi: 10.1890/06-0922.1. URL http://doi.wiley.com/10.1890/06-0922.1.

H. Gao, M. Hrachowitz, F. Fenicia, S. Gharari, and H. H. G. Savenije. Testing the realism of a topography-driven model (FLEX-Topo) in the nested catchments of the Upper Heihe, China. *Hydrology and Earth System Sciences*, 18(5):1895–1915, 2014. ISSN 16077938. doi: 10.5194/hess-18-1895-2014.

J. Hooghart and W. N. Lablans. Van Penman naar Makkink. Een nieuwe berekeningswijze voor klimatologisch verdamping getallen. Technical Report 19, KNMI, 1988.

G. Hu, L. Jia, and M. Menenti. Comparison of MOD16 and LSA-SAF MSG evapotranspiration products over Europe for 2011. *Remote Sensing of Environment*, 156:510–526, 2015. ISSN 00344257. doi: 10.1016/j.rse.2014.10.017.

R. Hurkmans and D. Klopstra. Bruikbaarheid Eact EUMETSAT. Technical report, HKV, 2015.

J. W. Kirchner. Getting the right answers for the right reasons: Linking measurements, analyses, and models to advance the science of hydrology. *Water Resources Research*, 42(3), 2006. ISSN 00431397. doi: 10.1029/2005WR004362.

P. Krause and D. P. Boyle. Advances in Geosciences Comparison of different efficiency criteria for hydrological model assessment. *Advances In Geosciences*, 5(89):89–97, 2005. ISSN 16807340. doi: 10.5194/adgeo-5-89-2005. URL http://www.adv-geosci.net/5/89/2005/.

A. Kunnath-Poovakka, D. Ryu, L. Renzullo, and B. George. The efficacy of calibrating hydrologic model using remotely sensed evapotranspiration and soil moisture for streamflow prediction. *Journal of Hydrology*, 535:509 – 524, 2016. ISSN 0022-1694. doi: http://dx.doi.org/10.1016/j.jhydrol.2016.02.018. URL http://www.sciencedirect.com/science/article/pii/S0022169416300439.

LSA SAF. Algorithm Theoretical Base Document, Down-welling Longwave Flux. Technical report, LSA SAF, 2009. URL http://landsaf.meteo.pt/GetDocument.do?id=298.

LSA SAF. SAF for Land Surface Analysis (LSA SAF) Algorithm Theoretical Basis Document. Evapotranspiration. Technical Report 1, LSA SAF, 2010. URL http://landsaf.meteo.pt/GetDocument.do?id=287.

LSA SAF. LSA SAF Validation Report Evapotranspiration (ET). Technical report, LSA SAF, 2011.

LSA SAF. Algorithm Theoretical Basis Document, Down-well Surface Shortwave Flux. Technical report, LSA SAF, 2012. URL http://landsaf.meteo.pt/GetDocument.do?id=469.

D. R. Maidment. *Handbook of Hydrology*. McGraw-Hill, New York, 1993.

W. M. L. Meijninger, F. Beyrich, A. Lüdi, W. Kohsiek, and H. A. R. D. Bruin. Scintillometer-Based Turbulent Fluxes of Sensible and Latent Heat Over a Heterogeneous Land Surface âĂŞ A Contribution to Litfass-2003. *Boundary-Layer Meteorology*, 121(1):89–110, oct 2006. ISSN

0006-8314. doi: 10.1007/s10546-005-9022-8. URL http://link.springer.com/10.1007/s10546-005-9022-8.

Ministerio de Agricultura Alimentación y Medio Ambiente. Sistema de Información del Anuario de Aforos, 2013. URL http://sig.magrama.es/aforos/.

Q. Mu, F. A. Heinsch, M. Zhao, and S. W. Running. Development of a global evapotranspiration algorithm based on MODIS and global meteorology data. *Remote Sensing of Environment*, 111(4):519–536, dec 2007. ISSN 00344257. doi: 10.1016/j.rse.2007.04.015. URL http://www.scopus.com/inward/record.url?eid=2-s2.0-35548929314{&}partnerID=tZOtx3y1.

J. Nash and J. Sutcliffe. River flow forecasting through conceptual models part I âĂŤ A discussion of principles. *Journal of Hydrology*, 10(3):282–290, apr 1970. ISSN 00221694. doi: 10.1016/0022-1694(70)90255-6. URL http://linkinghub.elsevier.com/retrieve/pii/0022169470902556.

Oak Ridge National Laboratory Distributed Active Archive Center (ORNL DAAC). FLUXNET, 2016.

D. Panagoulia. Assessment of daily catchment precipitation in mountainous regions for climate change interpretation. *Hydrological Sciences Journal*, 3(40):331–350, 12 1995.

D. Parr and G. Wang. Integrating remote sensing data on evapotranspiration and leaf area index with hydrological modeling: Impacts on model performance and future predictions. *Journal of Hydrometeorology*, 5(16):2086–2100, 10 2015.

F. Silvestro, S. Gabellani, R. Rudari, F. Delogu, P. Laiolo, and G. Boni. Uncertainty reduction and parameter estimation of a distributed hydrological model with ground and remote-sensing data. *Hydrology and Earth System Sciences*, 19(4):1727–1751, apr 2015. ISSN 1607-7938. doi: 10.5194/hess-19-1727-2015. URL http://www.hydrol-earth-syst-sci.net/19/1727/2015/hess-19-1727-2015.html.

R. E. Smith and R. H. B. Hebbert. A Monte Carlo Analysis of the hydrologic effects of spatial variability of infiltration. *Water Resources Research*, 15(2):419–429, apr 1979. ISSN 19447973. doi: 10.1029/WR015i002p00419. URL http://doi.wiley.com/10.1029/WR015i002p00419.

H. Stricker and W. Brutsaert. Actual evapotranspiration over a summer period in the âĂIJHupsel catchmentâĂİ. *Journal of Hydrology*, 39(1-2):139–157, oct 1978. ISSN 00221694. doi: 10.1016/0022-1694(78)90119-1. URL http://www.scopus.com/inward/record.url?eid=2-s2.0-0018024933{&}partnerID=tZOtx3y1.

T. E. Twine, W. P. Kustas, J. M. Norman, D. R. Cook, P. R. Houser, T. P. Meyers, J. H. Prueger, and M. L. Wesley. Correcting eddy covariance flux underestimates over grassland. *Agricultural and Forest Meteorology*, 103:279–300, 2000. ISSN 01681923. doi: 10.1016/S0168-1923(00)00123-4.

Y. van der Velde. *Dynamics in groundwater and surface water quality From field-scale processes to catchment-scale models*. PhD thesis, Wageningen University, 2011.

P. van Walsum, A. Veldhuizen, and P. Groenendijk. SIMGRO 7.1.0 Theory and model implementation. Technical report, WUR, 2010.

A. Veldhuizen. SIMGRO - complete integrated water model, 2016. URL http://www.wageningenur.nl/nl/Expertises-Dienstverlening/Onderzoeksinstituten/Alterra/Faciliteiten-Producten/Software-en-modellen/SIMGRO.htm.

Waterschap Online. Een kaart van ons gebied, 2016. URL http://waterschaponline.nl/reader/dna.php{#}browse/slide2.

K. Wilson. Energy balance closure at FLUXNET sites. *Agricultural and Forest Meteorology*, 113 (1-4):223–243, 2002. doi: 10.1016/S0168-1923(02)00109-0.

A. Wolf, N. Saliendra, K. Akshalov, D. A. Johnson, and E. Laca. Effects of different eddy covariance correction schemes on energy balance closure and comparisons with the modified Bowen ratio system. *Agricultural and Forest Meteorology*, 148(6-7):942–952, jun 2008. ISSN 01681923. doi: 10.1016/j.agrformet.2008.01.005. URL http://www.sciencedirect.com/science/article/pii/S0168192308000063.

L. Zhao, J. Xia, C. yu Xu, Z. Wang, L. Sobkowiak, and C. Long. Evapotranspiration estimation methods in hydrological models. *Journal of Geographical Sciences*, 23(2):359–369, apr 2013. ISSN 1009637X. doi: 10.1007/s11442-013-1015-9. URL http://link.springer.com/10.1007/s11442-013-1015-9.